Capacity of Concrete Beams Prestressed with BFRP Tendons

by

Sindri Hlífar Guðmundsson

Thesis
Master of Science in Civil Engineering with Specialization in Structural Design

June 2012

Capacity of Concrete Beams Prestressed with BFRP Tendons

Sindri Hlífar Guðmundsson

Thesis (30 ECTS) submitted to
the School of Science and Engineering
at Reykjavík University in partial fulfillment
of the requirements for the degree of

Master of Science in Civil Engineering with Specialization in Structural Design

June 2012

Supervisor:

Eyþór Rafn Þórhallsson
Associate Professor, Reykjavík University, Iceland

Examiner:

Torfi G. Sigurðsson M.Sc
General Manger at Mannvit Ltd

Ágrip

Titill á íslensku: Álagsþol steinsteyptra bita með forspenntum BFRP stöngum.

Steinsteypt mannvirki eru yfirleitt járnbent vegna lágs togstyrks steypunnar. Járnbending hentar að mörgu leyti vel en hefur þann ókost að tærast sé hún ekki varin. Þetta á einkum við þar sem raki, selta eða önnur efnaáraun er mikil. Við slíkar aðstæður geta önnur efni verið heppilegri sem bending t.d. trefjastangir (FRP) sem hafa verið reyndar víða um heim í þó nokkur ár með ágætis árangri. Basalttrefjastangir (BFRP) eru hinsvegar nýleg viðbót við trefjaefnin, þó svo þær hafi verið þekktar í áratugi. Basaltrefjar eru framleiddar úr basaltbergi sem er algengasta bergtegund heims. Þær hafa rúmlega tvisvar sinnum hærri togstyrk heldur en bendistál og eru léttar samanborið við styrk. Hinsvegar er fjaðurstuðullinn lágur 40-50 GPa samanborið við 200 GPa í bendistáli. BFRP stangirnar hafa því mikla toglengingu á fjaðursviði, sem myndi valda togsprungum í steyptum þversniðum. Til að nýta togstyrk stanganna betur án þess að steypan spryngi um of, er nauðsynlegt að spenna stangirnar.

Til að kanna vægiþol rétthyrnds steypuþversniðs, forspenntu með BFRP stöngum voru steyptir fjórir bitar sem síðan voru álagsprófaðir. Bitarnir voru án hefðbundinnar skerbendingar með hlutfall haflengdar á móti bendiarmi, (a/d) hlutfall 10,67. Fyrstu tveir bitarnir brotnuðu óvænt í samblandi af sker- og vægisbroti. Þá var ákveðið að styrkja seinni tvo bitana gegn skeri með utanáliggjandi stálhespum, sem voru klemmdar á bitana og þannig framkallað vægisbrot. Niðurstöður prófananna voru bornar saman við reikniaðferðir, sem flestar eru ætlaðar fyrir önnur trefjaefni eða stál sem bendingu. Aðferðunum fyrir útreikningum á vægiþoli bar vel saman við niðurstöður prófana en skerþolsjöfnur voru mjög á reiki. Þegar tilraunaniðurstöður voru bornar saman við niðurstöður fyrri tilrauna, kom í ljós að skerþol sama þversniðs með samskonar bendingu en helmingi lægra a/d hlutfalli, var tvöfalt hærra. Þetta undirstrikar að dreifing skerkrafta og beygjuvægis eftir hafinu, hefur áhrif á skerþol, þó að fæstar skerformúlur taki beint tillit til þess.

Lykilorð: Basalttrefjar, BFRP, forspenna, steyptir bitar, tilraun

Abstract

Concrete structures are usually reinforced because of its low tensile strength. A familiar reinforcing material is steel; it suits well as reinforcement but has a large drawback, corrosion. This is mainly a problem where structures are subjected to water, salty environment or other chemical actions. For those conditions other reinforcing materials are convenient i.e. fiber reinforced polymer (FRP), which has been used widely for several decades. Basalt fibers (BFRP) are a rather new material to structural design, although it has been known for several decades. They are made from basalt rock, are very light and have tensile strength, over twice as high as steel. BFRP has low elastic modulus 40-50 GPa compared to 200 GPa in steel, therefore its elastic lengthening is high, which induces cracking in concrete. To utilize BFRP tendons high strength and in order to prevent concrete cracking it is necessary to prestress them.

To investigate the moment capacity of BFRP prestressed concrete sections, four beams were casted, with shear span to depth (a/d) ratio of 10,67. They were tested under two point static loading. The first two beams failed due to a combination of shear and bending. Therefore it was decided to strengthen the other two agent's shear, with steel stirrups to get moment failure. Test results were compared to capacity calculation methods which usually are intended for other fibers reinforcement than basalt or for steel. Moment capacity methods agreed well but shear capacity methods varied. Test results were also compared to former research on beams with half the a/d ratio, but double shear strength. This difference of shear strength indicates that sherforce and bending moment distribution along the span have great influence on the failure mode, although capacity equations normally don't consider it directly.

Keywords: Basalt fiber, BFRP, prestress, concrete beams, experimental work

Capacity of Concrete Beams

Prestressed with BFRP Tendons

Sindri Hlífar Guðmundsson

Thesis (30 ECTS) submitted to
the School of Science and Engineering
at Reykjavík University in partial fulfillment
of the requirements for the degree of

Master of Science in Civil Engineering with Specialization in Structural Design

June 2012

Student: 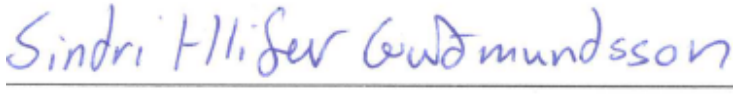

Sindri Hlífar Guðmundsson

Supervisor: 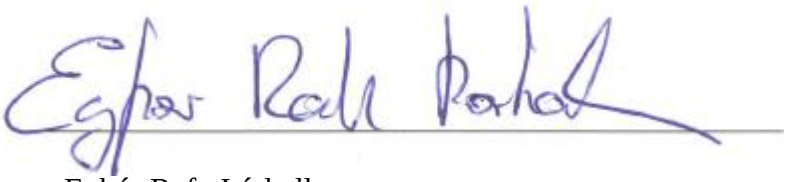

Eyþór Rafn Þórhallsson

Examiner: 

Torfi G. Sigurðsson

Acknowledgements

I would like to thank my supervisor Eyþór Rafn Þórhallsson, civil engineer M.Sc and associate professor at Reykjavik University for his help and guidance through this work.

Special thanks to all the people how help me with the experimental work and the thesis: Gísli Freyr Þorsteinsson technician at Reykjavik University, Indriði Ríkharðsson mechanical engineer M.Sc and assistant professor at Reykjavik University, Hrannar Traustason electronics engineer at Reykjavik University, Hafdís Dögg Hafsteinsdóttir librarian BA. at Reykjavik University, Eva Lind Ágústsdóttir civil engineer M.Sc at Icelandic Innovation Center, Hannes Garðarsson civil engineer M.Sc, Sigurður Jens Sigurðsson Urban planning and Transport engineer M.Sc, Áslaug Harpa Axelsdóttir industrial engineer M.Sc.

Contents

List of figures

List of tables

Notation

Roman upper case letters

A_C	Cross section area of concrete
A_f, A_{fl}, A_p	Cross section area of longitudinal fiber reinforcement
A_s	Cross section area of longitudinal steel reinforcement
$C_{Rd,c}$	Reduction factor, see EC2 – recommended value $0.18/\gamma_c$
E_c	Elastic modulus of concrete
E_f, E_p	Elastic modulus of fiber reinforcement
E_s	Standard elastic modulus of steel, taken as 200 GPa
F	Force
F_c	Compression force in concrete
F_f	Tension force in fibers
I_g	Sections moment of inertia
M_0	Service moment capacity
M_e	Moment due to tendons eccentricity
M_n , M_{ult}	Ultimate moment capacity
P	Prestress force
ΔP	Estimated loss of prestress force
V_c	Normal shear strength provided by concrete with steel flexural reinforcement
V_{cf}	Normal shear strength provided by concrete with FRP flexural reinforcement
$V_{Rd,c}$	Design shear resistance of member without shear reinforcement
$V_{Rd,c}$	Concrete contribution to the shear capacity
W	Section modulus
X	Distance from top to sections neutral axis
$\emptyset$	Diameter

Roman lower case letters

a	Shearspan of member
b_w, b_{beam}	Section wedge width
c	Depth from top to neutral axis
d	Effective depth of cross section
e, e_f	Eccentricity
f_c, f_{ck}, f_c'	Compressive strength of concrete
f_{ctm}	Mean tensile strength of concrete
f_{fu}, f_{pu}	Ultimate tensile strength of fibers
h, h_{beam}	Height of rectangular cross section
k	Factor, see EC2, chapter 6.2.2 and ACI 440.1R-06 ratio of depth of the neutral axis to the reinforcement depth
k_1	Factor equal to 0,15 according to EC2

Greek letters

β_1	Factor taken as 0,85 for concrete strength up to 27,5 MPa, which is reduced at a rate of 0,05 for each 6,9 MPa higher.
ε_{cu}	Ultimate compressive strain in concrete
ε_{ce}	Strain in concrete due to tendons eccentricity
ε_{ct}	Tension strain in concrete
ε_{fu} , ε_{pu}	Ultimate strain in tendons
ε_{pe}	Total strain capacity of tendon / strain in fibers due to prestress
υ_{min}	See EC2 chapter 6.2.2
ρ	Effective ratio of prestress / tension reinforcement ratio
ρ_b	Balanced reinforcement ratio
σ_{cp}	Compressive stress in concrete due to axial load or prestress
σ_e	Stress in concrete due to tendons eccentricity
τ_{rd}	Design shear stress

Abbreviations

FRP	Fibre reinforced polymers
AFRP	Aramid fibre reinforced polymers
BFRP	Basalt fibre reinforced polymers
CFRP	Carbon fibre reinforced polymers
RC	Reinforced concrete

1 Introduction

1.1 Background and problem statement

Concrete is a very familiar structural material and it is the most common structural material used in Iceland. It is relatively cheap and can usually be mixed quite near the construction site with limited transportation or shipping. Concrete has good compressive strength but rather low tensile strength, or approximately one tenth of its compressive strength. Therefore it is necessary to reinforce it and the most common way is by using steel. Reinforcing steel has high tensile strength, thermal expansion nearly the same as that of the concrete, is easy to handle and form, it can be welded and is very stable in production. These qualities as well as a relatively good price are among the things that make it so popular. However, it has a few limitations: corrosion, rather low fire resistance and its price has been rising. Normally, steel is protected from corrosion with some kind of coating e.g. paint or galvanization, but for reinforcing steel, concrete is the protection coating. This coating is manifested in the concrete cover which is normally 20-80 mm or even more in extreme cases. Concrete cover is determined in context with its environmental factors and use of the structure e.g. thick cover in salty environment or where higher fire resistance is required. At flexure this cover is of little use for the moment capacity but makes the cross section heavy, which is in most cases unfortunate and requires more reinforcement. It would be more economical to reduce the concrete cover and minimize cross sections that way, but to achieve that without reducing the durability of the structure the steel bars have to be coated, replaced by some other material or use chemical protection system (Bank, 2006). Since coatings are often expensive and have relatively short durability it is convenient to replace the steel reinforcement, usually by stainless steel or FRP bars (Fiber reinforced polymer). Both these materials are rather expensive compared to the usual reinforcing steel.

FRP reinforcing bars are made from long fibers (continuous) mainly glass carbon or aramid fibers. The fibers are “glued” together with polymer (resin) which is 40-80% of the volume (Bank, 2006). The FRP’s have been used for several decades as reinforcement for concrete but more commonly for fiber reinforcement, where short fibers are added to the concrete mixture. Fibers are also commonly used for strengthening sheets that are glued externally to the concrete, timber and even metal structures for repair or reuse. FRP bars have several advantages as reinforcement: very high tensile, high strength-weight ratio, do not rust, lightness and some fibers have thermal expansion/contraction similar to concrete. The main

disadvantages are: low compressive and shear strength, their brittle nature (have no plastic elongations), most types have low elastic modulus, some fibers can be damaged from ultraviolet light, high price and they can't be bent or welded.

For the last decade or so basal fibers (BFRP) have become more popular, which has been followed by research and testing of the material. Basalt fibers are made from ground basalt (rock) that is melted down and spun out to long fibers, with diameter of 12-18μm (Novitskii & Efremov, 2011). Thousands of fibers form the tendons and are "glued" together with resin similar to other FRP's. Basalt rock is very common in Icelandic nature, and research is ongoing about its suitability for production of fibers (Broddason, 2012).

Reykjavik University (RU) and the Icelandic Innovation Center (ICI) have done several researches in the past few years on the reinforcing ability of BFRP. The researches examine BFRP tendons both as reinforcement and sheets for strengthening among other things. Björgvin Smári Jónsson (Jónsson, 2011) did his master's thesis last year, where he tested BFRP as a prestressed bending for concrete beams. The main subject of his thesis was to compare calculated moment capacity and methods to the results of his specimen's beams. These beams were supposed to fail at flexure due to lower moment capacity than shear strength. But the experiment didn't go as planned because all specimen's beams failed at shear but not at moment as expected. Therefore, the main subject of this thesis is capacity, a comparison of calculated moment capacity versus tested.

Since BFRP is rather new material to structural engineering, design guidelines and codes are a bit lacking on that matter. There aren't many researches available containing BFRP as the reinforcing bars in concrete. However, a great deal of research has been carried out on strengthening of concrete with BFRP sheets.

BFRP has high tensile strength approx. 2,5 times that of reinforcing steel's, but low elastic modulus approximately ¼ of steel's. Therefore, it is convenient to prestress the BFRP tendons to use more of its high tensile strength. Thus moment and shear capacity can be induced due to the normal force in the section.

1.2 Aim of the study

The main aim of this study is to increase knowledge and proficiency about BFRP reinforced concrete, to estimate the efficiency of the BFRP tendons as reinforcement and evaluate the advantages and disadvantages. Furthermore to find some suitable load capacity calculation methods that could be used for prestressed BFRP tendons.

The main questions for this thesis, asked at the beginning are following:

- How much is the relaxation of BRFP tendons over a specific time?
- Do load capacity calculations methods, addressed in relevant codes and guides, agree with the experiment?
- What does this and former experiments reveal, regarding BFRP prestressed concrete?
- Is BFRP suitable to prestress concrete sections?

1.3 Objectives

The original plan was to carry out two experiments on the BFRP tendons, to test the relaxation of BFRP tendons stressed to consistent length and measure tendons strain loss over time. Two attempts were made to this experiment which both failed due to poor end connections (anchors) for the tendons. The second experiment contained moment capacity of concrete beams prestressed with BFRP tendons. This experiment was carried out and is listed in this thesis. Following are the objectives of the work:

1. Develop anchors for the BFRP tendons, so they can be prestressed.
2. Cast four identical beams prestressed with BFRP tendons. Same cross section as in a former experiment done by Björgvin Smári Jónsson.
3. Measure the strain in the tendons while the concrete is curing and at transfer to evaluate tendons relaxation.
4. Evaluate effective prestress force in the tendons after the transfer based on strain measurements.
5. Perform two point flexure test and measure moment capacity of the section. The capacity is measured at service due to crack widths and deflection. Ultimate moment capacity is measured at failure.
6. Compare measured moment resistance to calculated, according to codes and guides for FRP's and sometimes steel.
7. Compare these results to former results from Björgvin Smári Jónsson.

1.4 Scope of the work

The experimental work started late December last year, when the first attempt was made to measure the tendons relaxation. The second attempt was made in early January this year. After both those attempts failed a preparation started for prestressing tendons and casting the beams. The tendons were prestressed on 22 February 2012 and beams casted the day after. The beams were tested in two sections on 23-24 of Mars 2012 and 13 of April. After finishing the experimental work, the data was analyzed and the report finished.

This thesis is organized into an introduction and other six main chapters that are outlined below:

Second chapter: Brief and general discussion about the methodology that was used, focusing on experimental setup and how former research will be used.

Third chapter: Properties of FRP and prestress reviewed as well as flexural and shear strength of concrete beam sections.

Fourth chapter: Preparation and setup of experimental work, equipment modifications and general description of experiment setup.

Fifth chapter: Results from experimental work and related discussion.

Sixth chapter: Discussion about the whole work, cooperation of results from the experiment, calculations and former experiments. Recommendations for further researches are addressed.

Seventh chapter: The whole work summarized and conclusions drawn.

Material properties and detailed calculations are listed in appendixes.

Expected end of this work is at the end of May 2012 and graduation is on June 9th of 2012.

2 Research methodology

2.1 Introduction

This thesis is somewhat a continuation from Björgvin Smári Jónsson's thesis: *Prestressed BFRP tendons in concrete beams,* from last year at Reykjavík University. The aim of his experiment was to test concrete beams reinforced with prestressed BFRP tendons. This method simulates precast one way slabs that are often prestressed. His experimental work consisted of: casting four concrete beams b*h*L = 200*200*2000 mm, three prestressed with two Ø 10 mm BFRP tendons and one with un-prestressed BFRP reinforcement. These beams were tested in a two point flexural test to check their moment capacity due to static loading. The BFRP specimen's beams failed unexpectedly at shear. Björgvin reviewed many shear formulas and compared calculated shear strength of the section, according to these formulas with measured shear strength from the experiment. The calculated shear strength was varied between individual formulas. The main conclusions that he drew from the study were:

- *"Ultimate bearing resistance of a beam with prestressed BFRP tendons is not much higher than of un-prestressed beams but the SLS bearing resistance is much higher and the deflection is smaller.*
- *The long-term relaxation (100 year) is estimated around 20%. That is comparable with aramid fibers but much higher than for steel and carbon fibers.*
- *Special care should be taken when designing members without shear reinforcement."*

(Jónsson, 2011, p. 55)

This ultimate bearing resistance was limited to shear failure. Therefore it was decided to try again a similar experiment setup, but with longer beams that would fail at bending and compare those results with simulating calculations.

The longtime relaxation was formulated from strain loss in the BFRP tendons over a period of 19 days while the concrete was curing. Because the tendons were located in the concrete as reinforcement, the concrete heat effect and moisture affected the results. Like Björgvin pointed out it would be better to measure strain in BFRP tendons separately from the concrete.

2.2 Experimental work

To evaluate the relaxation of the BFRP tendons it was decided to stretch two tendons to a consistent length due to 50% of its ultimate tension strength, and measure its strain loss over one month or so. The strain loss would be measured with strain gauges connected to the tendons and longtime relaxation calculated according to those measurements. It would be more reliable to measure relaxation over a longer period but master's theses have limited time. This experiment would also give a chance to test new anchors for prestressing BFRP tendons. Anchoring BFRP tendons for prestress has been rather difficult due to the fact that the tendons can't be clamped or welded. A solution to this problem has been developed at Reykjavik University, that is similar to the one used in this project. It was decided to cast four beams b*h*L = 200*200*3860 mm for the two point flexure test (Figure 2-1).

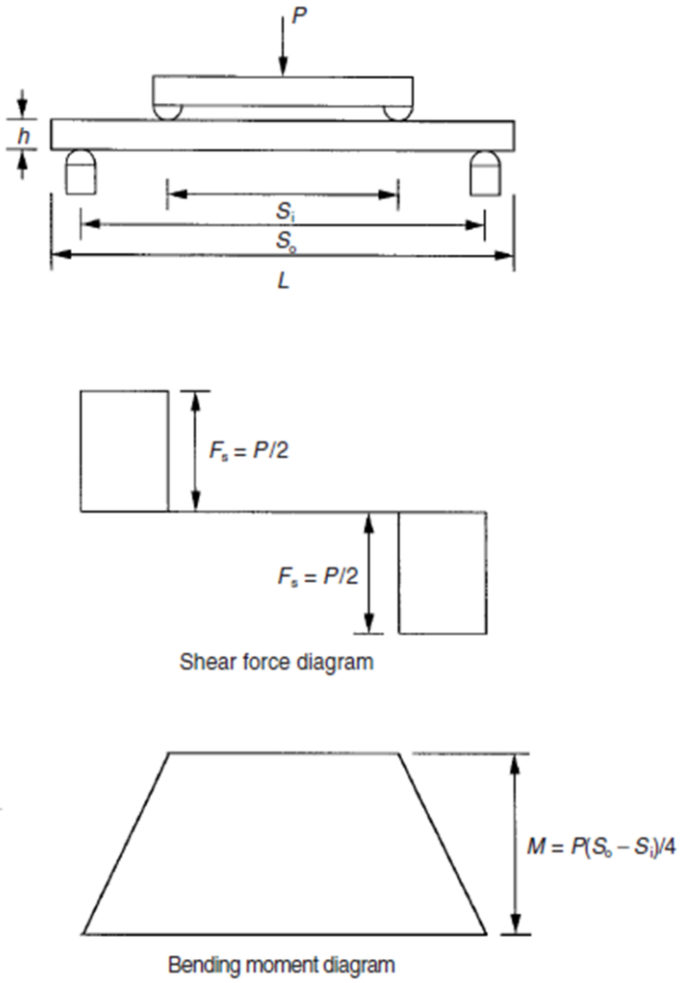

Figure 2-1 Two point flexure test, shear force and bending moment diagram (Hodgkinson, 2000)

Each beam was reinforced with two Ø 10 mm BFRP tendons that were available in a 4 m length. At least, three beams were needed for the experiment to get trustworthy results and because of possible errors in strain gauges one beam was added for safer results. Variability of concrete specimens is often the case, therefore it would have been more reliable to have additional samples but because of limited time and equipment it was decided to have just a minimum number of samples. Beams were prestressed, casted and tested at RU's lab with the available equipment that needed some modifications in most cases.

Tendon's strain was measured while prestressing and until after transferring to evaluate effective prestress force and have some record of tendon's relaxation. Two point bending test was used to measure their moment capacity (Figure 2-1), were each beam undergoes static loading until failure. Distance between loading points on top of the beams has to be wide enough so the middle part of the beams is free of shear force. However as this distance goes wider the shear force gets higher and the bending moment lower, therefore it needs to be balanced. Strain was measured in each beam at concretes extreme compression fibers, at the tension zone and at tendons. With those measurements the strain could be modeled for the cross section where high moment occurs. Force and displacement was measured automatically and collected. It was more difficult to measure cracks in the concrete because no available equipment could handle that automatically. Therefore, crack widths had to be estimated at the early stages of testing for each beam. Crack widths were used as a scale for serviceability limit state (SLS) load capacity as well as displacements.

Special research was carried out to evaluate strain gauges accuracy, the error turned out to be less than 4%. Further information for this test is listed in appendix D. The jacking force equipment was tested with standard press at ICI and the result showed a small error for which measurements of this thesis experimental work were corrected.

2.3 Simulating calculations

Since basalt is a rather new material in structural engineering, design guidelines and codes are a bit lacking. Therefore, available calculations methods are limited to other FRP's and steel. Those calculations are all "hand" calculations based on static methods in codas, guides and design books. Computer simulations are not used in this thesis because elastic simulations aren't realistic for this project and inelastic simulations need software that take more time to handle.

3 Literature review

3.1 Introduction

This chapter contains background information about topics relevant to this thesis research and experimental work. FRP's are briefly introduced with emphasis of BFRP and its abilities as internal reinforcement in concrete. Former researches are reviewed as well as appropriate designing codes for FRP reinforced concrete. Relevant capacity calculations methods are introduced for FRP's both in shear and flexure.

3.2 FRP

Composite materials or composites, consist of at least two different materials which combined make the resulting composite material that is different from the original materials (GangaRao, Taly, & Vijay, 2007). A typical combination of materials in composites is fibers and polymer (resin) this combination is often referred to as *fiber reinforced polymer* or FRP. The continuous fibers, with high strength are the backbone of the composite material and reinforce the polymer matrix. Fibers are bound together with polymeric matrix which also has the purpose to protect the fibers from damage, from fabrication until the end of service life and to transfer stresses to the fibers (*FRP reinforcement in RC structures*, 2007). There are a few types of fibers that are most familiar: aramid FRP (AFRP), carbon FRP (CFRP), and glass FRP (GFRP). The use of basalt FRP (BFRP) has become more common in the past decade or so but isn't nearly as common as the other three. These FRP's have different advances and dis-advances e.g. varying production cost, tensile strength, elastic modulus etc. (Table 3-1).

Table 3-1 Usual properties of FRP reinforcing bars (ACI 440.1R-03, 2003, p. 9)

	Steel	GFRP	CFRP	AFRP
Nominal yield stress, ksi (MPa)	40 to 75 (276 to 517)	N/A	N/A	N/A
Tensile strength, ksi (MPa)	70 to 100 (483 to 690)	70 to 230 (483 to 1600)	87 to 535 (600 to 3690)	250 to 368 (1720 to 2540)
Elastic modulus, $\times 10^3$ ksi (GPa)	29.0 (200.0)	5.1 to 7.4 (35.0 to 51.0)	15.9 to 84.0 (120.0 to 580.0)	6.0 to 18.2 (41.0 to 125.0)
Yield strain, %	1.4 to 2.5	N/A	N/A	N/A
Rupture strain, %	6.0 to 12.0	1.2 to 3.1	0.5 to 1.7	1.9 to 4.4

*Typical values for fiber volume fractions ranging from 0.5 to 0.7.

All these FRP's have relatively low elastic modulus and high tensile strength parallel to fibers. The main advances are: high tensile strength to self-weight ratio, 10-15 times greater than that of steal and good corrosion resistance. The main disadvantages are low elastic modulus (except some CFRP's), lack of ductility, low shear strength and issues in alkaline environments (Waldon, 2005).

Aramid Fibers were originally produced under the trade name Kevlar, which was the first generation of FRP prestressing tendons in the 1980's. Their moisture absorption, low melting temperature, high price and relatively poor compressive properties made them less interesting for FRP parts of constructions. AFRP's are light weight compared to other fibers and have high energy absorption due to relatively high rupture strain and damping coefficient.

Carbon Fibers do not absorb moisture like the AFRP's and can stand more heat. Their thermal coefficient is negative or very low, which makes them suited for extreme temperatures in some cases. They are durable and have relatively high tensile strength which makes them attractive for FRP parts of structural engineering application.

Glass Fibers are sensitive to moisture, especially in salt and alkali environment. They are also sensitive to creep rupture under sustained stress and therefore, the strength is reduced to 60% of ultimate in some cases. Relatively low cost, high chemical resistance and excellent insulating properties make GFRP attractive to use in FRP parts of construction (Bank, 2006; *FRP reinforcement in RC structures*, 2007).

The reinforcing fibers for rebars and sheets are continuous (very long) unlike fibers that are used in hot tubs and boats. Reinforcing fibers are very small with a typical diameter of 3-25 μm and therefore there are thousands of continuous fibers in one rebar (Jónsson, 2011). The fibers lay parallel to the rebar; are "glued" together or filed up with matrix which is available in several types: polyester, vinyl ester and epoxy, each type having many sub types (Okelo & Yuan, 2005). Epoxy resins have excellent corrosion resistance and less shrinkage than others when curried. Polyester matrixes have good environmental properties and durability but have high shrinkage when curried. Vinyl ester matrix combines advances of the other two having good environmental abilities and is more flexible. It is a hybrid of epoxy and polyester resin which combined, have good abilities and is generally replacing polyester matrixes (Bank, 2006; *FRP reinforcement in RC structures*, 2007).

Fire resistance of reinforced concrete (RC) concrete section is highly subjected to their reinforcement heat resistance. Some fibers can stand high temperature, but FRP's fire resistance is mainly depending on the matrix resins. Sumida, Atsushi and Mutsuyoshi, Hiroshi released an article (2008) about testing of RC concrete beams with carbon and aramid FRP bars where heat resistant resin was used. Flexure test was carried out on these concrete beams which gave promising results. Resistance was higher with the new resin than regular and beams reinforced with carbon fiber bars were compatible with steel reinforced beams (Sumida & Mutsuyoshi, 2008).

FRP's have been used for many years to strengthen structures, either for repair to get former strength or to meet up with new use of the structure. Two popular methods are near-surface mounted (NSM) reinforcement and externally bonded sheets. For NSM, reinforcement bars or

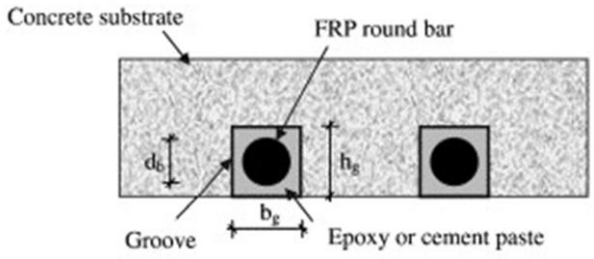

Figure 3-2 Schematic sketch of NSM reinforcement (De Lorenzis & Teng, 2007)

strips are grooved into the surface of the concrete (Figure 3-2). Bars are often prestressed to use more of its high tensile strength (De Lorenzis & Teng, 2007). Cracking load incises as well as former reinforce yield strength (Nordin & Täljsten, 2006). Increased crack load reduces the risk of corrosion due to less access of water which also reduces the risk of freeze-thaw influence on concrete.

Figure 3-1 Confined column (Konráðsson, 2011)

FRP sheets (Figure 3-1) have been widely used for strengthening of concrete structures for the past two decades or so. They are used e.g. to increase durability, to strengthen up structures for new loading requirements or structures that have been damaged, also to increase resistance for seismic loading (Bank, 2006).

3.3 BFRP

Basalt fibers are a rather new material to structural engineering although they have been known for nearly a century. They have become more popular for the past decade or so as a reinforcement fiber in polymer matrix (FRP). Basalt fibers have been used in fiber reinforcement for concrete directly and as FRP, both internal reinforcement as rebars and external with sheets (Figure 3-3).

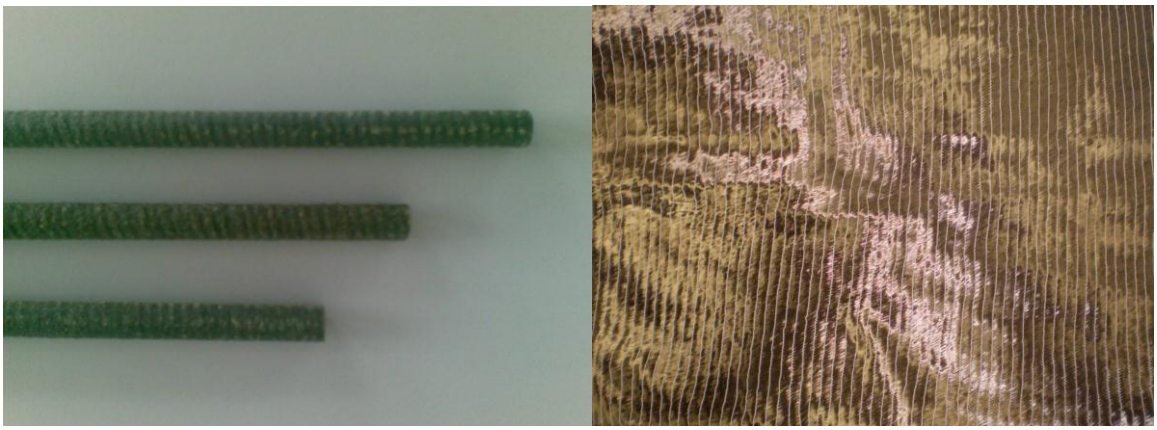

Figure 3-3 (Left) Sand coted BFRP rebars. (Right) Basalt sheets

Basalt is the most common rock type in the world (Ramakrishnan & Panchalan, 2005). Basalt fibers are produced by melting the rock at 1400-1600°C and are formed into 5-15 μm thick fibers (Ágústsdóttir & Sveinsdóttir, 2010). Basalt fibers are compatible with other fibers e.g. aramid glass and carbon, both in production cost and mechanical properties. They have good chemical ability, are environmentally and ecologically harmless, have no bad reactions to water and are not flammable (Jónsson, 2011). Basalt fibers are also very light 2,6 g/cm^3, have high tension strength parallel to fibers ~ 2500 MPa, have high heat resistance and are non-corrosive. The main disadvantages are: low elastic modulus, low shear strength compared to tension strength, their longtime durability hasn't been proven, they can't be welded nor clamped and they can't be shaped after production, which makes installing difficult in some cases (Arya, Clarke, Kay, & O'Regan, 2002).

Although basalt fibers have high heat resistance and can be used over wide temperature range from about -260/-200 to about 650/800°C, the resin loses its strength at much lower temperatures and loses its ability to transfer stresses in the fibers (Kiekens, Van de Velde, & Van Langenhove, 2003). Jingyu Wu, Hui LI & Guijun Xian, 2010 tested thermal effects on BFRP rebars with regular polymer matrix and sand coated surface. The testing temperatures were from room temperature to 350°C and results showed that rebars tensile strength was

almost the same from room temperature to 250°C. After the temperature rose over 250°C the tensile strength dropped rapidly, or 40% at 300°C and 70% at 350°C. The experiment shoved also that tensile strength dropped less than 10% when specimens were kept at 250°C for 8 hours' time. This shows that BFRP starts losing its tensile strength due to lower heat than regular reinforcing steel, which is one of the most significant drawbacks of BFRP. As previously pointed out some tests are ongoing with heat resistant resin that could give better results.

Bonding between basalt rebars and concrete has been a problem. Therefore, modern rebars from some manufacturers are coded with sand, which makes the surface like sandpaper. Other manufacturers have made ribs on the surface similar to reinforcing steel (Ágústsdóttir & Sveinsdóttir, 2010).

Since BFRP is a rather new material in structural engineering, there is a lack of experience regarding its durability. In a research done by Hui Li et al., 2011 the freeze-thaw resistance of BFRP rebars and strips with epoxy resin was tested. The temperature range was -30°- +30°C in a 24 hour period. Results showed that after 88 cycles there was no degradation on tensile properties. They also carried out research on BFRP mechanical properties due to immersion ageing. The samples were immersed in distilled water and alkaline solution. Both rebars and strips showed remarkable decrease in tension properties. Another Chinese research shows similar results (Li, Xion, Xiao, & Wu, 2010). Durability of BFRP is mainly depending on the resin, both its long term properties and how it protects the fibers (Banibayat, 2011). BFRP mechanical properties vary between manufacturers and must be taken with great care.

3.4 Prestress

Normally concrete is strong in compression but weak in tension. Although reinforcement is used to take up the tension which concrete can't resist, it cracks in its tension zone. By prestressing, the concrete section is set under compression, which reduces the section's tension force due to flexure and therefore cracks (Figure 3-4). The crack control is significant for concrete because of less access of water into the section which leads to corrosion in steel reinforcement, less durability of FRP's and increased freeze-thaw effects. Spans can be increased by applying prestress and slabs can be thinner (Bhatt, 2011).

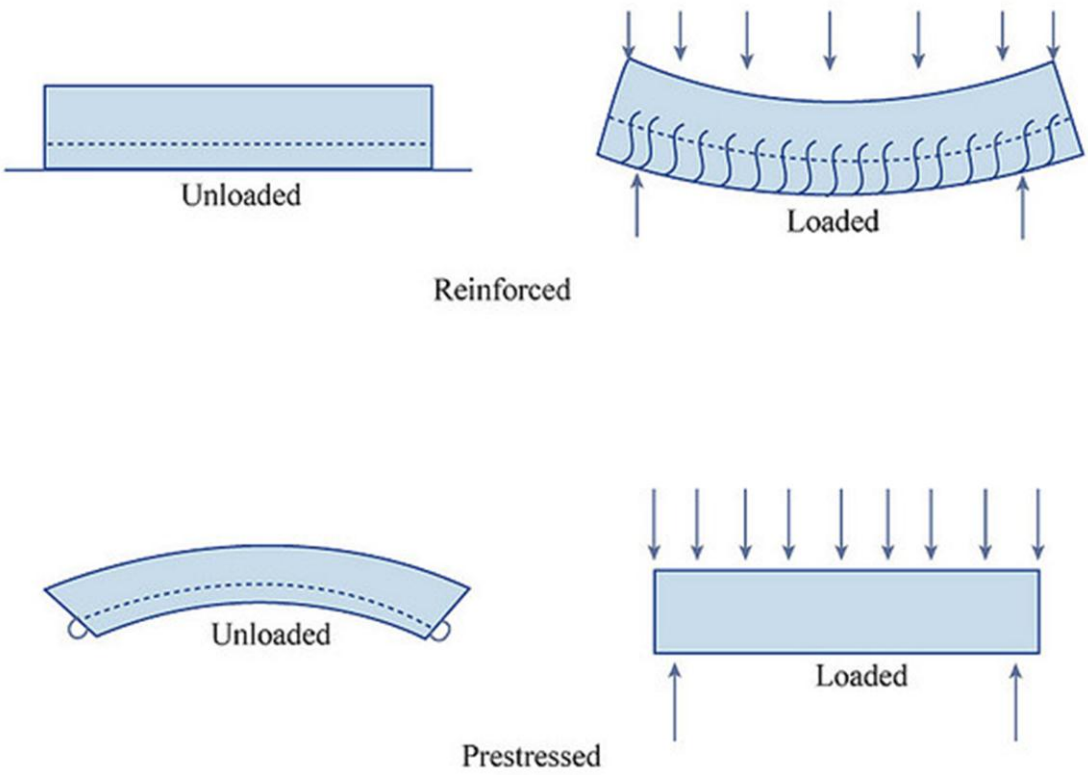

Figure 3-4 Schematic picture of reinforced and prestressed concrete (OpenCourseWare, 2008)

As seen on Figure 3-4 the loaded prestressed beam is in level and therefore, tensile stresses acting on the section are reduced. The stress distribution can be seen in Figure 3-5.

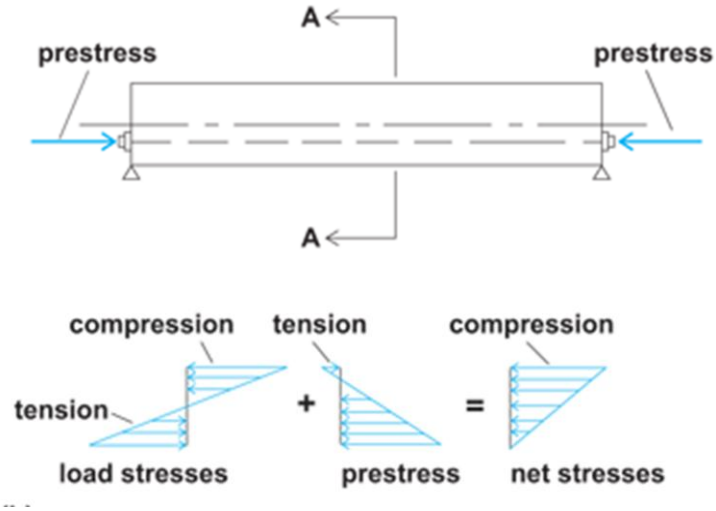

Figure 3-5 Stress distribution for prestressed concrete section (Ghaffar, 2008)

The low elastic modulus of BFRP rebars leads to large deformation of members which doesn't necessarily affect the flexural performance, but affects the serviceability criteria. Concrete has very limited deformations ability without cracking and therefore is BFRP high

tension strength of little use, when it is used as internal reinforcement. By prestressing BFRP tendons, its tension abilities are utilized and the service load of the structure increased. Normally, FRP tendons are prestressed to 40-65% of their ultimate tensile strength, compared to typical prestressing force of steel, 85% of its yield strength (ACI 440.4R-04, 2004).

Prestressed tendons are most commonly used in precast structural elements where special equipment (stressing bed) is used to stress the tendons before casting. When concrete has cured to the desired strength level, the prestress load is transferred from the stressing bed to the concrete member. At this stage, tendons want to return to their unstressed state but are prevented by concrete because of grip between tendons and concrete (Bhatt, 2011). When tendons don't have enough pull out strength like some FRPs, anchoring tendons at the ends become necessary. Anchors are also used as a grip for the stressing equipment. Usually anchors for steel cables are threaded or conic so they clamp the cable when stressed. Both these methods are unsuited for BFRP tendons, as well as some other FRP's because of lacking compressive strength especially perpendicular to fibers and the fact that FRP's simply can't be threaded. Therefore anchoring is still a weak link of FRP's (Bank, 2006). In the experimental work of this thesis chemical anchors are used, which are explained in chapter 4.

3.5 Losses in prestress

Prestressing force is subjected to losses both at transfer and after prestressing load is applied to the member. For normally prestressed concrete with steel cables, losses occur because of following cases:

- Elastic shortening of concrete.
- Creep of concrete under sustained compression (long time effects).
- Relaxation of prestressing steel under sustained tension (long time effects).
- Shrinkage of concrete (long time effects).

(W.H, Bungey, & Hulse, 2007)

When anchors are used some additional losses can be expected at transfer due to slipping. When all losses have been added up it can be 25% of the original jacking force (Bhatt, 2011).

According to the (ACI 440.4R-04, 2004), which is the American code for prestressed structures with FRP tendons (not BFRP), the losses due to elastic shortening of concrete, creep and shrinkage can be calculated using standard methods for concrete sections

prestressed with steel. Elastic modulus of FRP tendons should be used instead of steel tendons. It is also revealed that:

"*Losses for FRP tendons due to these three sources are typically less than the corresponding losses for steel tendons due to the lower modulus of elasticity of FRP tendons. Relaxation losses are more problematic and are less well understood, as there is little experimental data available that describes relaxation loss profiles for FRP tendons*" (ACI 440.4R-04, 2004, p. 14).

Many factors affect the losses of FRP's e.g. type of fiber, type of resin matrix and ratio, applied prestress force and length of member. There is rather little information or research available regarding prestress losses of BFRP, which is unfortunate.

3.6 Shear of FRP reinforced beams

In RC structures, shear is still partly unsolved and no analytical methods are currently available. Concrete's shear strength calculation methods are therefore based on empirical data from test results (W.H et al., 2007). When shear load on concrete section is larger than the section shear resistance, additional transvers reinforcement is needed to resist the load. Often there are requirements of minimal shear reinforcement (stirrups) in concrete sections although shear load is little. Tests show that there are many types of shear failures for beams, usually shear cracks develop from vertical flexural cracks but when shear force is large compared to bending moment shear cracks are more "clean" inclined or diagonal cracks (Bhatt, 2011). The diagonal shear strength of concrete sections is a combination of several things: shear strength of the concrete's untracked compression area, friction between the concrete on each side of the critical crack (aggregate interlock) and the vertical component of the shear force that the main tensile reinforcement carries (dowel action) (Bank, 2006).

The shear strength of concrete members reinforced with FRP's is lower than with steel reinforcement, as the following text shows.

"*The shear strength of flexural concrete members with FRP longitudinal reinforcement and no shear reinforcement has indicated a lower shear strength than a similarly steel-reinforced member without any shear reinforcement. Due to the lower strength and stiffness of FRP bars in the transverse direction, their role toward dowel action is also expected to be less than that of an equivalent steel area*" (GangaRao et al., 2007, p. 248).

Considering simple beam section. Because of FRP's low elastic modulus, the depth of neutral axis is less than for steel reinforcement. Therefore there is less untracked concrete area, which reduces the shear strength. The flexural stiffness of FRP reinforced beams is lower than that of reinforced steel, therefore critical diagonal cracks can be wider. FRP's have lower transvers strength than steel and are less stiff (Bank, 2006). Therefore shear resistance formulas for steel reinforced concrete can't be used directly for FRP reinforced concrete. Some general aspects about shear cracks and mechanisms can be seen on Figure 3-6 and 3-7.

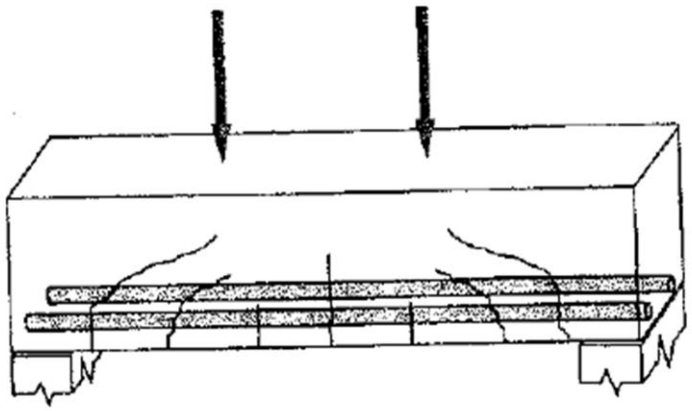

Figure 3-6 Shear cracks in beam with longitudinal reinforcement

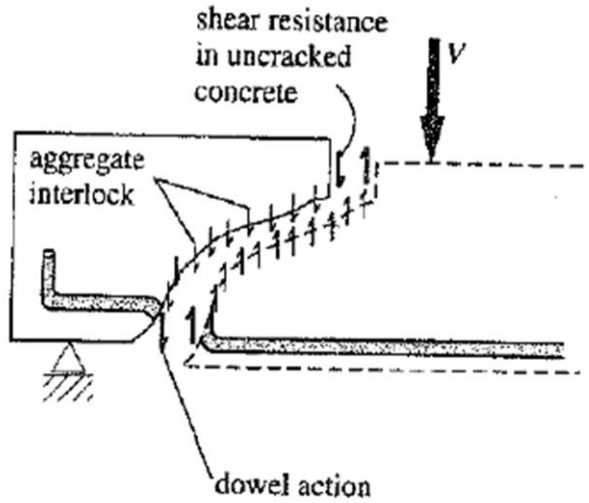

Figure 3-7 Mechanisms of shear transfer (Jónsson, 2011, p. 14).

Jónsson, 2011 reviewed several shear capacity formulas in his thesis (Table 3-2). He calculated shear capacity of 200*200 mm concrete section with cylinder strength of f_{ck} 50 MPa which was reinforced with two BFRP tendons, whose tensile strength was 1200 MPa.

The cross section of his experimental specimens is identical to the experimental specimen cross section used in this thesis. These formulas were both intended for steel and FRP reinforcement and both for imperial and SI units but the shear strength is listed in kN. It is noted whether the equation is for steel or FRP and where it is published.

Table 3-2 Comparing shear capacity of concrete beams without shear reinforcement (Jónsson, 2011, p. 19).

Shear strength	KN	Steel/FRP	Code	Formula
V_c	38,7	Steel	ACI 318-08	$V_c = \left(\frac{\lambda \cdot \sqrt{f'_c}}{6}\right) \cdot b_w \cdot d$
V_c	33,3	Steel	EC2:2004	$V_{Rd,c} = (C_{Rd,c} \cdot k(100 \cdot \rho_l \cdot f_{ck})^{1/3} + k_1 \cdot \sigma_{cp}) b_w \cdot d$
$V_{c,min}$	33,6	Steel	EC2:2004	$V_{Rd,c} = (v_{min} + k_1 \cdot \sigma_{cp}) b_w \cdot d$
V_c	22,7	Steel	EC2:2004	$V_{Rd,c} = (C_{Rd,c} \cdot k(100 \cdot \rho_l \cdot f_{ck})^{1/3}) b_w \cdot d$
$V_{c,min}$	23,0	Steel	EC2:2004	$V_{Rd,c} = v_{min} \; b_w \cdot d$
V_{cf}	2,9	FRP	ACI 440.1R-03	$V_{c,f} = \frac{\rho_f \cdot E_f}{90 \cdot \beta_1 \cdot f'_c} \cdot V_c$
V_{cf}	10,9	FRP	ACI 440.1R-06	$V_c = 5 \cdot \sqrt{f'_c} \cdot b_w \cdot c$
V_{cf}	13,7	FRP	CNR-DT 203	$V_{Rd,ct} = 1{,}3 \cdot \left(\frac{E_f}{E_s}\right)^{1/2} \cdot V_{Rd,c}$
V_{cf}	18,5	FRP	fib40(EC2)	$V_{cf} = 0.12 \cdot (1 + \sqrt{\frac{200}{d}}) \cdot (100 \cdot \frac{A_f}{b_w \cdot d} \cdot \frac{E_f}{E_s} \cdot \phi_e \cdot f_{ck})^{1/3} \cdot b_w \cdot d$
V_{cf}	31,4	FRP	fib40(ACI)	$V_{cf} = V_c \cdot (\frac{E_f}{E_s} \cdot \phi_e)^{1/3}$
V_{cf}	**29**	**FRP**	**EC2(fib 40)**	$V_{Rd,c} = (C_{Rd,c} \cdot k\left(100 \cdot \rho_l \cdot \frac{E_f}{E_s} \cdot \phi_e \cdot f_{ck}\right)^{1/3} + k_1 \cdot \sigma_{cp}) b_w \cdot d$

The last equation (in bold) is Jónsson's modification of the EC2 (2004) equation for steel where ratio between elastic modulus of steel and BFRP is taken into account as well as the ratio between allowed strain for the same materials. This modification fitted his experimental results nicely. It can be seen that equations intended for steel reinforcement give higher shear strength than FRP equations. The (ACI 440.1R-03, 2003) equation is the oldest one and gives the lowest shear strength, and actually raises the shear strength as the equation gets younger. Only the Eurocode 2 equations (2 and 3 from the top) utilize axial force to increase shear strength and these equations are for steel reinforcement. All the other equations neglect these effects of axial force on the section. It should also be noted that these FRP equations are for carbon-, glass- and aramid fibers, none of these equations are designed for BFRP. These

equations are generally not designed especially for FRP reinforced concrete, just modification of former equations for steel reinforcement (*FRP reinforcement in RC structures*, 2007). Therefore, further researches are needed to evaluate how well these equations follow the actual result of BFRP reinforced concrete.

3.7 Flexural shear

Formally discussed shear capacity equations only consider shear but neglect the effects of bending moment. Generally when a beam is subjected to loading that induces shear forces and bending moments, the behavior depends on the distribution of shear force and bending moment along the beam (Figure 3-8). This makes the shear calculations even more complex (Bhatt, 2011). The crack development for beams where shear forces and bending moments interact can be described as follows: inclined shear cracks in webs of RC beams either develop as extensions of vertical flexural cracks (flexure-shear crack) or as independent cracks (*web shear*). Flexure-shear cracks occur because of combination of bending moment and shear force that leads to tension stresses perpendicular to 45° line with beams' axes. (McCormac & Brown, 2009).

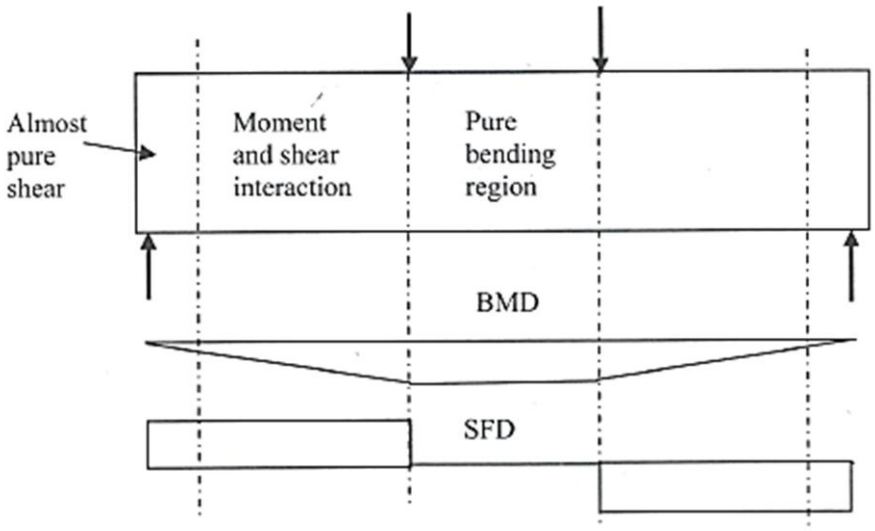

Figure 3-8 Beam under two point loading (Bhatt, 2011, p. 193).

In research carried out by Nehdi, El Chabib, & Saïd, 2007 results for tested shear capacity of 168 FRP reinforced concrete beams were collected. They used genetic algorithms to calculate coefficients for a semi empirical equation developed by Zsutty, 1971 for steel reinforcement without stirrups. The equation was modified for FRP reinforcement by the ratio between FRP and steel's elastic modulus. These were beams with normal strength concrete, shear span to

depth ratio of 1,8-6,5 and longitudinal reinforcement ratio times FRP's elastic modulus of 0,3-3,2. Data for beams without shear reinforcement were 68 which the resulting equation fitted quite nicely.

The resulting equation with modified coefficients:

$$V_{cf} = 2{,}1\,(\frac{f_c \rho_{fl} d}{a}\frac{E_{fl}}{E_s})^{0{,}3} b_w d \qquad for \frac{a}{d} > 2{,}5 \qquad \textbf{(3-1)}$$

$$For \frac{a}{d} < 2{,}5\ , V_{cf}\ is\ multiplied\ by\ 2{,}5d/a$$

Where:

b_w is the beam wedge width.

d is the beam effective depth.

a is the beam shear span.

f_c is cylinder strength of concrete.

E_{fl} is elastic modulus of tensile FRP reinforcement.

E_s is standard elastic modulus of steel, taken as 200 GPa.

$\rho_{fl} = \frac{A_{fl}}{b_w\, d}$ is the longitudinal reinforcement ratio.

The calculated shear capacity of the beam specimen in this thesis, according to equation (3-1) is 12,5 kN which is similar to the Italian guide (CNR-DT 203, 2006) value 13,6 kN. This Italian equation is modified steel reinforcement equation for FRP by taking the ratio between elastic modulus and other coefficients to reduce the capacity.

What separates equation (3-1) from other shear equations, is the shear span length which is considered. In this way beams with shorter shear span have a higher shear capacity than beams with a longer shear span. It has been shown that failure mode of rectangular RC beam is strongly depending on the a/d ratio. In a research carried out by Ramadass & Thomas, 2010 on beams reinforced with GFRP rebars and modeled according to ACI 440.4R-04, 2004. This model showed that beams having a/d ratio less than 9 filed in shear.

In should be noted that these equations consider other FRPs than BFRP, although they are used as such.

3.8 Flexure

The ultimate moment capacity of reinforced concrete depends on a combination of concrete compressive strength and reinforcement's tension strength. When the concrete section is lightly reinforced, compared to the large compressive zone of the section, is it considered under-reinforced. These sections have larger plastic deformation prior to collapse, which gives a warning before failure. This quantity makes the ductile failure mode highly desirable for design. When sections have a large area of tensile reinforcement present compared to a small compression zone of concrete, the section is considered to be over-reinforced. The failure mode of this section is brittle, due to crushing of the concrete in compression. Since failure occurs sudden and brittle, is it considered as unacceptable failure (O'Brien, Dixon, & Sheils, 2012). Since FRPs are fully elastic, failures modes of under-reinforced sections are due to tendon rupture, brittle and sudden. Therefore an over reinforced section is more desirable, although failure due to concrete cursing is brittle and sudden, it is somewhat less brittle than FRP rupture (Bank, 2006). Over reinforcement is a more uneconomical design, due to over amount of FRPs. The lack of ductility in FRP reinforced sections makes them undesirable for structures where seismic loading can be expanded (Figure 3-9).

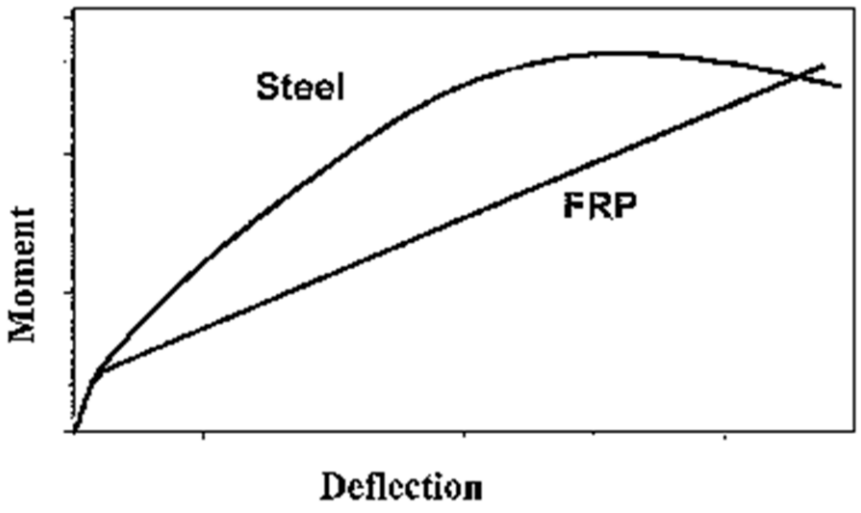

Figure 3-9 Schematic representation of moment-deflection responses of prestressed concrete elements (ACI 440.4R-04, 2004, p.14)

FRP reinforced structures don't absorb energy as steel reinforced structures with their plastic displacements. But the elastic displacements are higher in FRP reinforced structures, although large displacements incise cracking of concrete (Sharbatdar & Saatcioglu, 2009).

So far, only the ultimate capacity of concrete sections has been discussed, but in structural design two stages have to be considered. Firstly there is serviceability limit states (SLS) which is applied to ensure a structure's functionality and integrity under service conditions. In these stages stresses, deflections and crack widths are checked to ensure appropriate requirements. The main difference between FRP and steel reinforcement is the stress limit of FRP due to durability and creep rupture. Some codes have reduction factors for FRPs stresses because of that, but these factors are usually intended for some other fibers than basalt. Crack widths for steel reinforced concrete structures is 0,3 mm according to Eurocode 2 (EN 1992-1-1, 2004). For a simple rectangular prestressed beam stresses due to service load can be calculated by adding together stresses from all load components (Figure 3-10). The tension stresses are of more interest than compression stresses due to concrete cracking. For prestressed members with eccentricity of tendons it is also necessary to check tension stresses due to eccentricity without load, in order to predict cracks.

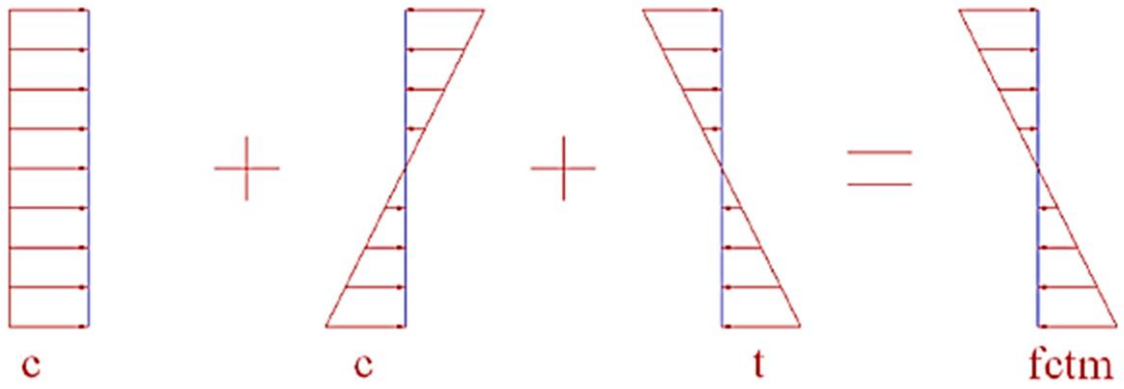

Figure 3-10 Stress in prestressed concrete section due to: compression force, tendon eccentricity, applied load = mean tensile strength of concrete (Jónsson, 2011, p.41)

Crack widths may be incised for FRP reinforced concrete due to corrosion free material but environmental conditions need to be considered as well, e.g. effects of alkali and freeze-thaw.

Secondly there is ultimate limit state (ULS) were structures must be able to withstand collapse. Since this thesis is undertaking simple beam, only ultimate moment capacity and shear which was reviewed in the last section are considered.

The ACI Committee has a standard for prestressed FRPs (ACI 440.4R-04, 2004) which illustrate calculation methods for moment capacity of those sections. The approach is based on the concept of balanced design where concrete reaches its ultimate compression strain as well as fibers (Figure 3-11).

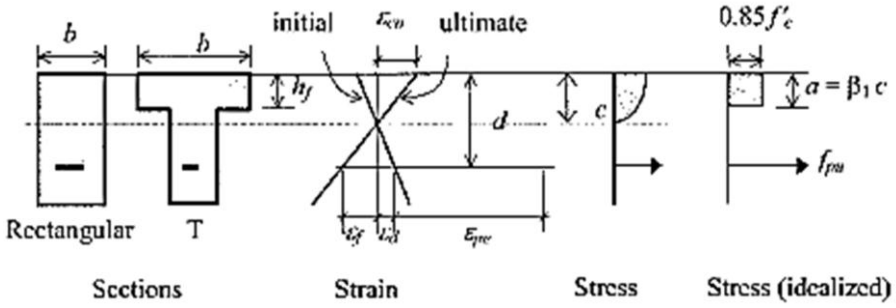

Figure 3-11 Balanced section, strain and stress conditions (ACI 440.4R-04, 2004, p. 14)

The balanced radio ρ_b is calculated with the following equation:

$$\rho_b = 0{,}85\beta_1 \frac{f_c'}{f_{pu}} \frac{\varepsilon_{cu}}{\varepsilon_{cu} + \varepsilon_{pu} - \varepsilon_{pe}} \quad \textbf{(3-2)}$$

Where $\beta_1 = 0{,}85$ for concrete strength up to 27,5 MPa, which is reduced at a rate of 0,05 for each 6,9 MPa higher.

f_c' is concrete compressive stress.

f_{pu} is tendons ultimate tensile stress.

ε_{cu} is concrete ultimate compressive strain.

ε_{pu} is the amount of strain available for flexure.

ε_{pe} is the total strain capacity of tendon, less than used for prestress.

When the balanced radio ρ_b is known it is compared to tension reinforcement radio ρ which is calculated by:

$$\rho = \frac{A_f}{b_w d} \quad \textbf{(3-3)}$$

Where:

A_f is area of FRP tension reinforcement.

b_w and b are beams with four rectangular sections.

d is beams effective depth.

For reinforcement ratios ρ less than balanced radio ρ_b, that is $\rho \leq \rho_b$, is the beam strength governed by tendon tensile strength (tension controlled section). A rectangular stress block of concrete is assumed, although concrete compression zone hasn't reached its strain limit. This assumption produces less than 3% error compared to an elastic analysis of the cracked section.

The moment capacity is calculated by:

$$M_n = \rho\, b\, d^2 f_{pu}\left(1 - \frac{\rho}{1{,}7}\,\frac{f_{\rho u}}{f_c'}\right) \quad \textbf{(3-4)}$$

For reinforcement ratios ρ is higher than balanced radio ρ_b, that is $\rho \geq \rho_b$, is the beam strength governed by the concrete compressive strength (compression controlled section). A rectangular stress block of concrete is assumed and a linear elastic behavior of tendons. The tendons strain is defined and neutral axis location. The moment capacity is calculated by summing moments about the tendon location.

$$M_n = f_c'\, b\, \beta_1 k_u\, d^2\left(1 - \frac{\beta_1 k_u}{2}\right) \quad \textbf{(3-5)}$$

Where $k_u = c/d$ ratio and c is depth from top to neutral axis.

The Canadian standard (CSA) has a similar approach for moment capacity calculations of prestressed sections. There is as slight difference in handling of tension controlled sections, were rectangular stress block is not used directly. Coefficients are adjusted to represent concrete compressive strength (ISIS Education Committee, 2007). The Concrete Society has calculation methods for moment capacity but they don't consider prestressed sections (*FRP reinforcement in RC structures*, 2007). The same can be said for the Italian standard (CNR-DT 203, 2006).

This thesis's experimental section is nearly balanced and rectangular stress block assumed. Therefore moment capacity can be calculated with a usual method for prestressed sections. In *Reinforced and prestressed concrete design* by O'Brien et al., 2012 a calculation method is listed for a prestressed section according to (EN 1992-1-1, 2004). This method considers a balanced section where concrete compression force and tendons tension force are calculated according to its strain limits.

Strain in concrete ε_{cu} due to tendons eccentricity is calculated with the following equation:

$$\varepsilon_{cu} = \frac{1}{E_c}\left(\frac{\rho P}{A_c} + \frac{\rho P e_f^2}{I_g}\right) \quad \textbf{(3-6)}$$

Where:

E_c is concrete modulus of elasticity.

A_c is beam cross section area.

I_g is section gross moment of inertia.

P is prestress force acting on the section.

ρ is effective ratio of prestress.

e_f is tendon eccentricity.

Concrete strain at tension ε_{ct} is calculated with the following equation:

$$\varepsilon_{ct} = \frac{-\varepsilon_{cu}(d - x)}{x} \quad \textbf{(3-7)}$$

Where:

ε_{cu} is concrete ultimate compressive strain.

d is the beam effective depth.

x is cross sections' natural axis location, solved from these equations.

Strain in tendons $\varepsilon_{fu}$is calculated with the following equation:

$$\varepsilon_{fu} = \frac{-\rho\ P}{A_f E_f} - |\varepsilon_{ct}| - |\varepsilon_{ce}| \quad \textbf{(3-8)}$$

Where:

E_f is tendon modulus of elasticity.

A_f is tendon cross section area.

Tendon tension force F_f and concrete compression force F_c are then calculated:

$$F_f = A_f E_f |\varepsilon_{fu}| = F_c = 0{,}8\ x\ b\ 0{,}85 f_c \quad \textbf{(3-9)}$$

Finally ultimate moment capacity M_{ult} is calculated by:

$$M_{ult} = F_f\ (d - 0{,}4x) \quad \textbf{(3-10)}$$

These equations are designed for steel prestressed concrete sections, but force mechanism in sections due to bending is very similar for FRP prestressed sections.

Moment capacity calculations are listed in appendix F.

4 Experimental work

4.1 Introduction

The main idea was to cast four beams prestressed with two BFRP tendons each, and check their moment resistance. The experimental work took place at the engineering laboratory in Reykjavík University (SEL) late December 2011 until early April 2012. The main experiment was to check moment resistance of the beams (Figure 4-1), but previous tests were carried out for the anchor and strain gauges to check if they worked properly for the main experiment. Those experiments are listed in appendix C and D. The main experiment is listed in this chapter and the equipment adjustments needed. Detailed work is listed in appendix E.

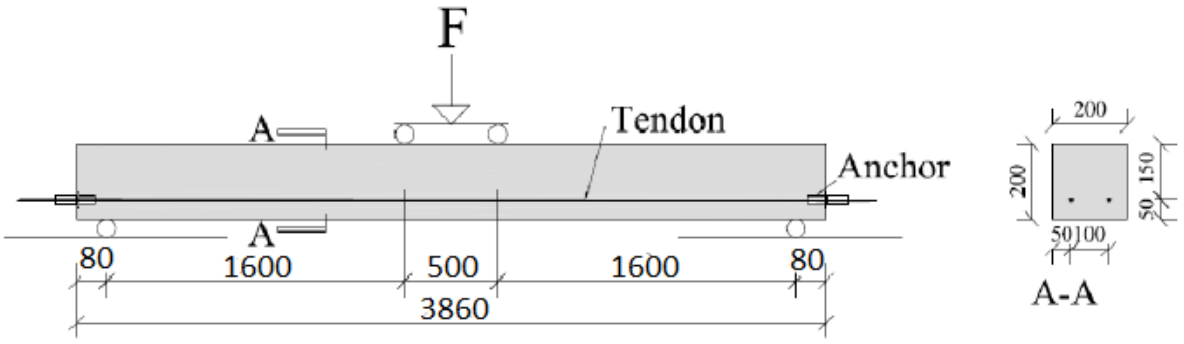

Figure 4-1 Schematic drawings of bending test setup and beam cross section

Expected load capacity (F) for the beam due to flexural failure:

F_{servis} = 14,7 kN

$F_{ultimet}$ = 35,1 kN

Detailed calculations are listed in appendix F.

4.2 Equipment for prestress

All four beams had to be cast at the same time and from the same concrete mixture, to get them as homogenous as possible. Therefore it was necessary to have them all prestressed at the same time. Available equipment at the lab was unable to perform this operation without quite a bit of modifications. Therefore it was decided to make new equipment from scratch suitable for this purpose (prestress bench).

The new prestress bench consists of two angle sections (“L” shaped) h*b*t = 200*200*20 mm spaced 4070 mm apart so the BFRP tendons could be stressed between them (Figure 4-2). The angle sections were bolted to a concrete floor with 8 glued “HILTI HIS-N M12” (“Hylse med indv gevind HIS-N M12X125: Varenr.: 00258017,” n.d.).

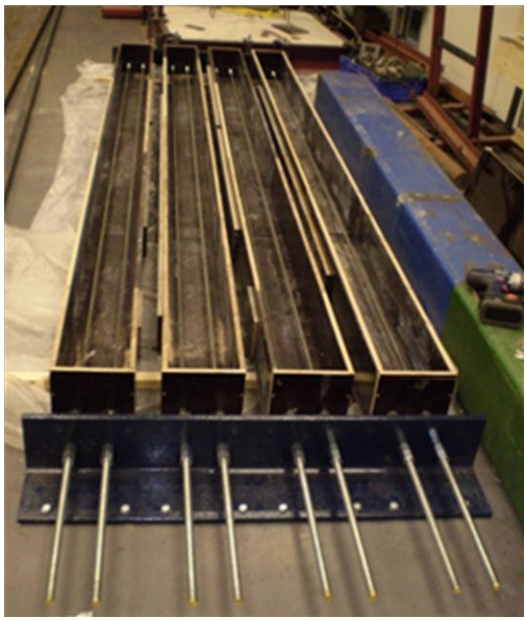

Figure 4-2 New prestress bench (blue painted angel sections)

4.3 Anchors

The BFRP tendons can’t be clamped or welded in the ends to induce fastening to the prestress bench (end blocs). That problem has been solved at RU at least for experimental testing and used for several experiments on BFRP tendons. The solution is to glue the BFRP tendons in to a steel tube with “Hilti HIT-RE” concrete glue (“Klæbemørtel HIT-RE 500/330/1: Varenr.: 00305074,” n.d.). The steel tubes are screw threaded inside to induce contact between the concrete glue and the steel. This solution has functioned well but doesn’t suite when there are more than two beams prestressed at the same time. Therefore a brand new version of anchors was developed and used for this experiment. Those new end blocks together with the new prestress bench would enable all eight tendons to be prestressed individually at the same time.

The new version of end blocks was simply M 20 mm stainless steel threaded rod. An Ø 11 mm hole was drilled 150 mm into its end and threaded with M 10 thread 100 mm in from the end. The threaded surface induces contact between the steel and the glue, and therefore it is very important to clean all oil from the surface in contact with the glue.

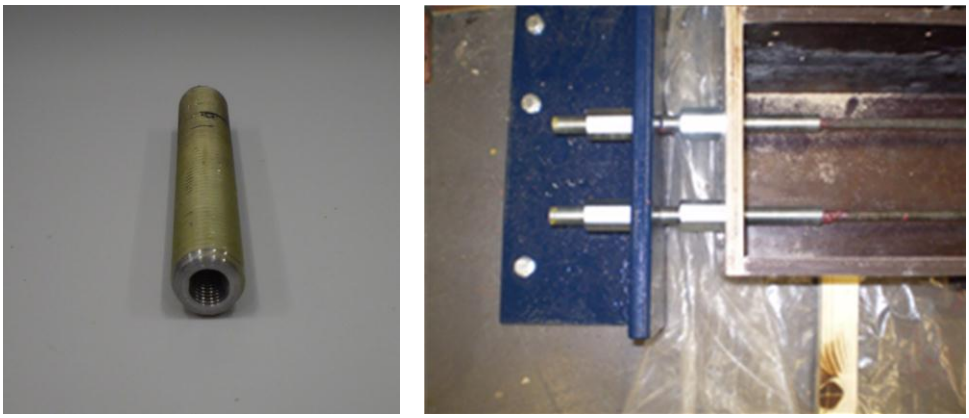

Figure 4-3 (Left) Anchor ready to use. (Right) Anchor installed to prestress bench

The BFRP tendons were then glued into the threaded steel rods (anchor) which were of two different lengths for each end of the BPRP tendons, 270 mm for the fixed end and 730 mm for the jacked end. Each anchor was laid through 20,5 mm diameter hole on each of the angle shapes and tightened up with a nut (Figure 4-3). Another nut was installed between the concrete beam and the angle shapes on each anchor, that will be tightened to the beam when the concrete has gained its compression strength. That way prestress force is moved from the prestress bench to the concrete beams.

4.4 Formwork

To outline the concrete at casting it is necessary to have reliable form work. In this case a 16 mm thick oil coded plywood was used that was screwed together and formed beam outline h*b*l = 200*200*3860 mm (Figure 4-4). On the joint of individual plywood plates, another layer of plywood was installed to stiffen the connection. The forms had two Ø 35 mm holes on each end, so the tendons could lay out and be connected to the prestress bench. To preclude slipping of the tendons, a washer was installed at the ends of the formwork and would then resist on the beams ends after transfer. The washers were made from h*b*t = 60*200*6 mm steel and had two Ø 20 mm holes for the rods. The forms were leveled and fastened to the prestress bench.

Figure 4-4 Form work

4.5 Strain gauge

Strain gauges were used to measure the strain in the BFRP tendons. The gauges consist of fine girded metal wires that elongate or shorten with the tendon and measure strain proportional to the elongation of the tendon. As the length of the wires changes the electrical resistance changes as well. The strain is calculated according to the electric resistance. Since the gauges are electrical, it is important to protect them from water, as well as the electrical wires connecting them to the computer. If water or some other conductive material comes into contact with the electric wires, it would distort the results. Therefore, the sensors were wrapped with insulating tape and coated with "Sikaflex 15LM" which is a low-modulus sealant ("Building Sealants," n.d.). The electric wires were laid in Ø 6 mm plastic tubes that lay from the gauges and out through the bottom of the forms and connected to a computer device (Figure 4-5).

Figure 4-5 (Left) Upper strain gauge is wrapped with insulating tape which has been coded with sealant over the tape on the lower tendon. (Right) Computer device for strain measuring

Tendon strain was measured continuously from prestress until after transfer when gauges were unplugged to move the beams. Strain measurements at the tendons were continued for each beam at flexural testing, furthermore three other gauges were installed on each beam: two 30 mm long gauges on the beams top face, in the middle 50 mm from the sites and one 50 mm long gauge on the beams site in level with the tendons (Figure 4-6). These gauges had the purpose of measuring strain in the concrete at extreme locations, compressive strain at the beams top face and the tensile strain in level with the tendons. Although maximal tension strain occurs at the bottom face of the beam, it was decided to locate the gauge in level with tendons for comparisons. Strain measurements were collected with a computer device every two seconds.

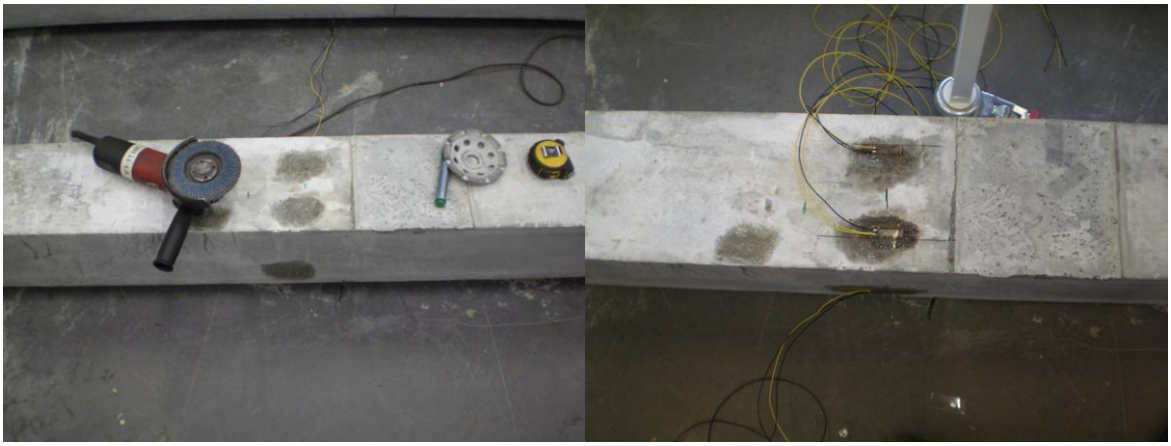

Figure 4-6 (Left) Beam prepared for gauges (Right) Beam with installed gauges

4.6 Prestress

The decided prestress rate was 50% of the BFRP tendon tensile strength, which corresponds to 600 Mpa tensile stress and 47 kN prestress force per tendon. The recommended prestress rate is 40-65% for FRP tendons, while typical prestress rate of steel is 85% of its yield strength (ACI 440.4R-04, 2004; Bank, 2006). The BFRP tendons would elongate approximately 45 mm due to this prestress force. Hydraulic jack was used to prestress the tendons and the force was measured simultaneously with a computer device that calculates and collects the force due to the oil pressure in the jack (Figure 4-7). The tendons were prestressed in three relays to keep the force destitution in the prestress bench as even as possible and furthermore to minimize the relaxation of tendons due to movements in the bench. Once the jack had reached its decided force the nut on the corresponding anchor was tightened to the prestressed bench to keep consistence force until transfer. Strain gauges measured the strain in the tendons while prestressing.

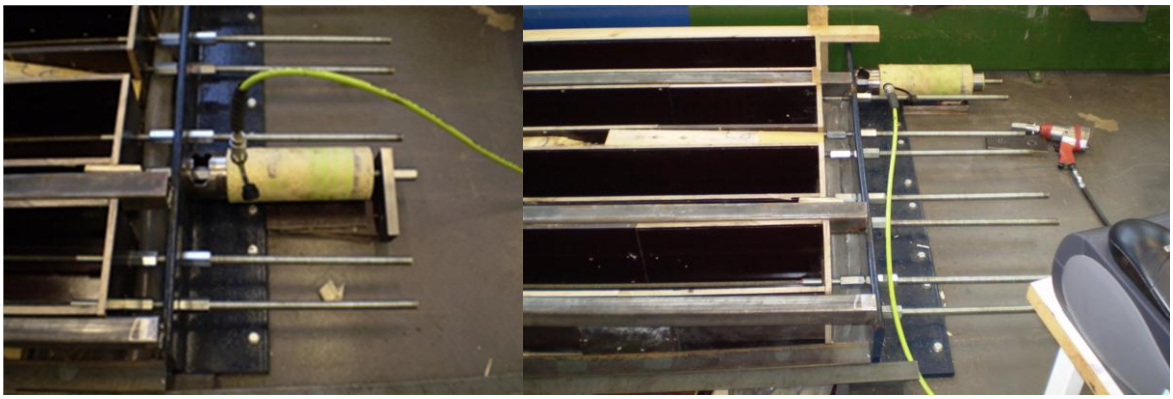

Figure 4-7 Prestressing the tendons with a hydraulic jack

4.7 Concrete and casting

All four beams were casted from the same concrete mixture that was bought from BM Vallá. The concrete strength class was 50 MPa cylinder strength, and with the maximum grain size of 19 mm. The concrete mixture details (listed from producer) are shown in appendix B. The concrete lorry delivered the concrete at RU's lab and it was transported from the truck to the forms in a wheelbarrow (Figure 4-8). At casting the concrete was picked to make sure it was compact. To minimize surface cracks in the concrete, the beam top surface was watered 10 hours after casting and a couple of times a day for a week after (Figure 4-9). The top surface was also covered with a plastic sheet. Average heat in the lab while the concrete was curing was 20°C and humidity 30%.

Figure 4-8 Concrete casting

Figure 4-9 (Left) Piking concrete and (right) beams covered with a plastic sheet

4.8 Transfer

The prestress force was transferred from the prestress bench to the beams 24 days after casting and taken out of the form work the day after. Tendon strain was measured at transfer to estimate the prestress losses. Because of the heaviness of the beams, 370 kg, they had to be moved with a fork lift in the lab. Also because of the beam low depth, long span and tendon eccentricity they had to be lifted on the ends to prevent negative stresses in the beam top fiber. Those movements were done very carefully to prevent crack in the concrete (Figure 4-10).

Figure 4-10 (Left) Cutting off extra anchor for prestressing jack. (Right) Moving beam with forklift

4.9 Equipment for bending test

The beams were tested at two point load induced by hydraulic jack. The force bench "Hallgerður Langbók" was used for the flexure test with some modifications (Figure 4-11). This force bench consists of 8 m long RHS 300 profiles bolted to the concrete floor. The concrete beams sat on Ø 50 mm steel cylinders in the ends on top of the RHS profile. Large deflection of the concrete beam at flexure was expected, so there had to be enough space underneath the beams in the middle. Therefore, the beams were lifted up by installing HEB 200 between the steel cylinders and the RHS profile on both ends. The hydraulic jack was bolted to a HEB 100 steel beam fitted to four M20 threaded steel rods which transferred the load to the RHS 300 profile. HEB 140 steel beam was used to distribute the one point load from the hydraulic jack to two points on top of the concrete beams. Two steel cylinders Ø 50 mm spaced 500 mm apart, were used to transfer the load from the HEB profile to the concrete beams. The spacing between the cylinders was kept as small as possible to reduce the shear

force and increase beams bending moment. All four steel cylinders could rotate, but horizontal movements along the beams were restrained.

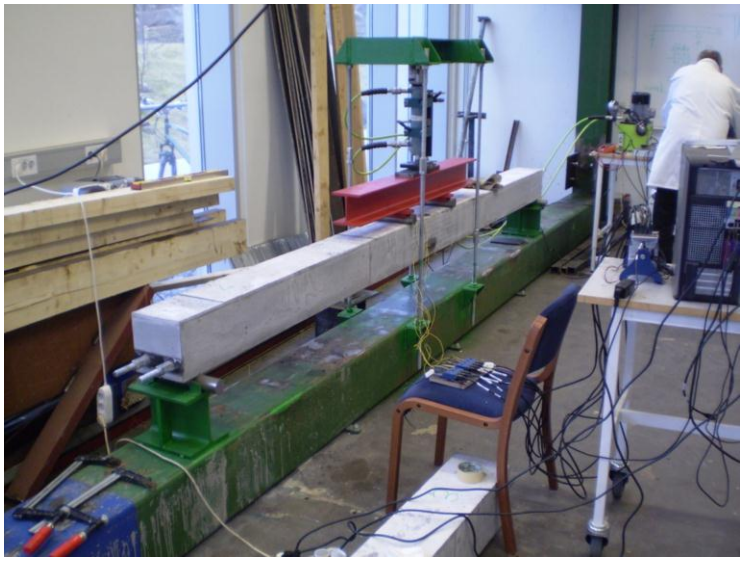

Figure 4-11 Beam in flexural testing

The available jacking equipment wasn't capable of keeping the force increment nor the displacement standard. However, to keep some control of the loading speed, the hydraulic pump rotation speed was set to a constant. Therefore, loading speed decreased as the load increased. Jacking speed was kept as low as possible to simulate static loading. The jack was spaced at the center of the concrete beams and the steel cylinder supports were spaced 80 mm from the ends of the beams, 3700 mm apart (Figure 4-1). The jack force was measured automatically with a computer device due to the hydraulic pressure in the jack. Measurements were collected in every 11/64 of a second as well as displacement of the jack.

On the last beam tested, vibration measurements with special measuring equipment were tried out. These measurements showed vibration as a function of time for two sensors in opposite directions. Development of new concrete cracks and tendon rupture was seen this way by pulse of vibration. Unfortunately there were some troubles with the data so it couldn't be used.

4.10 External stirrups

Two beams were fitted with external stirrups to prevent shear failure. These stirrups consisted of UNP 65 steel profile on top of the beam and under, bolted together with two M 10 bolts (Figure 4-12).

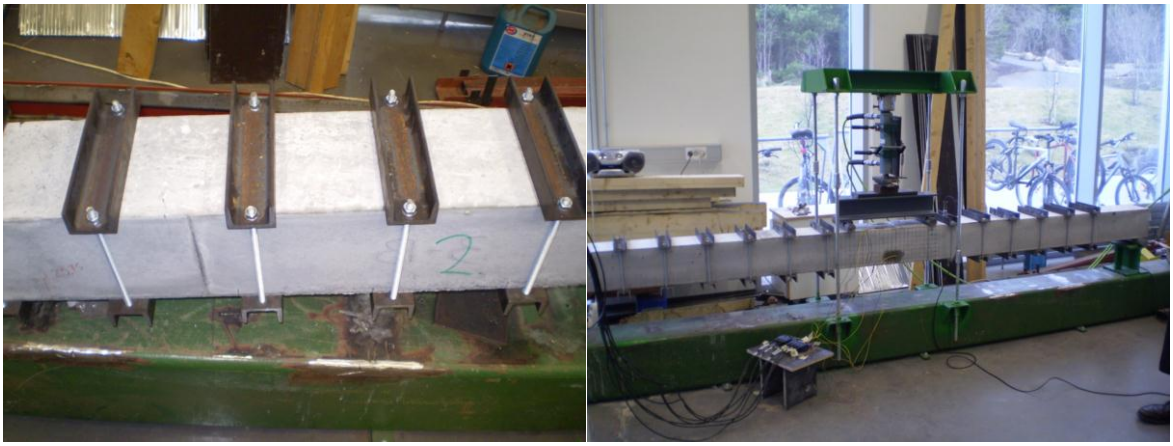

Figure 4-12 External steel stirrups fitted to beam

Twelve stirrups were fitted to each beam, six on each side of the jack spaced 210 mm apart, and first stirrup was located 500 mm from end. Nuts were tightened with a torch of 600 kg*cm.

4.11 Cylinder specimen

Six cylinders were cast simultaneously with the beams. They were of standard size “smaller” d*h = 100*200 mm, according to standard procedure (ÍST EN 12390-3). The standard cylinder strength corresponds to d*h = 150*300 cylinders. Therefore it is necessary to multiply smaller cylinder strength by 0.95 to get the standard strength. The cylinders were taken out of the forms six days after casting and wrapped in a cellophane and plastic sheet (Figure 4-13). Specimens were stored at the lab under the same heat and humidity conditions as the beams to correspond to their concrete strength. Beams were tested in relays and three cylinder specimens were tested for each relay. The specimens were tested at Innovation center of Iceland (ICI) in a standard cylinder specimen press. These first three specimens that correspond to beams 3 and 4, had the mean compressive strength of 57,1 MPa (Table 4-1) and the second three specimens correspond to beams 1 and 2 with cylinder strength of 65,2 MPa (Table 4-2).

Table 4-1 Cylinder specimens for beams 3 and 4

Casting day 23.2.2012 Test day 26.2.2012 Concrete age 32 days

Diameter mm	Area mm^2	Length mm	Volume mm^3	Weight kg	Vol.weight ton/m^3	Load kN	Strength Mpa
100,5	7933	200	1,59,E+06	3,84	2,42	500	59,9
100,0	7854	200	1,57,E+06	3,76	2,39	449	54,3
100,0	7854	200	1,57,E+06	3,77	2,40	471	57,0
				Mean:	2,40	**Mean:**	**57,1**
						Std.	2,79

Table 4-2 Cylinder specimens for beams 1 and 2

Casting day 23.2.20012 Test day 18.4.2012 Concrete age 55 days

Diameter mm	Area mm^2	Length mm	Volume mm^3	Weight kg	Vol.weight ton/m^3	Load kN	Strength MPa
100,4	7920	200	1,58,E+06	3,82	2,41	563	67,5
100,7	7962	200,8	1,60,E+06	3,93	2,46	542	64,6
100,7	7967	200,2	1,59,E+06	3,83	2,40	532	63,4
				Mean:	2,42	**Mean:**	**65,2**
						Std.	2,13

Cylinder failure was rather brittle because of high concrete strength (Figure 4-14).

Figure 4-13 (Left) Cylinder specimens 100*200 mm. (Right) Specimen covered in plastic

Figure 4-14 Specimens after testing

4.12 Modulus of elasticity

Elastic modulus of concrete was calculated according to table 3.1 (EN 1992-1-1, 2004) where

$$E_{cm} = 22 * (\frac{f_{cm}}{10})^{0,3}$$

and concrete mean tensile strength was calculated according to the same table where

$$f_{ctm} = 2{,}12 * \ln\left(1 + \left(\frac{f_{ctm}}{10}\right)\right)$$

for concrete strength over C50/60. Results of these calculations are listed in Table 6-1.

Sound measurements were carried out on beams to verify the beam modulus of elasticity. Measuring instrument from CNS Instruments Ltd. was used. This instrument transmits pulse

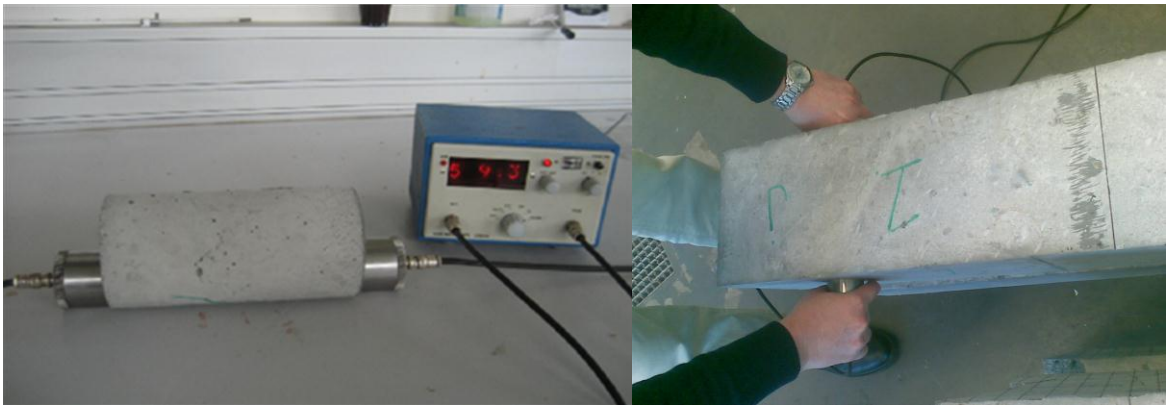

Figure 4-15 (Left) Instrument set up. (Right) Measuring beam 1

waves from one sensor to another and measures the travel time (Figure 4-15). When the travel time is known and the beam thickness, the longitudinal wave velocity, V_L and modulus of elasticity, E can be calculated with the following equation:

$$E = \frac{V_L^2 * \rho(1+\upsilon) * (1-2\upsilon)}{1-\upsilon} \quad \textbf{(4-1)}$$

Where ρ is the material density and υ is the material Poisson's ratio taken as 0,2. Results for measurements on modulus of elasticity are listed in Table 4-3.

Table 4-3 Measurements of modulus of elasticity

1,00E-06 1,00E-03

Beam no.	**Time ms**	**Distance mm**	**Velocity m/s**	**Poisson's ratio**	**Density kg/m^3**	**E GPa**
1	43,7	198,9	4551	0,2	2400	44,7
1	43,4	200,4	4618	0,2	2400	46,1
2	43,9	199,1	4535	0,2	2400	44,4
2	43,5	200,3	4605	0,2	2400	45,8
3	43,0	199,3	4635	0,2	2400	46,4
4	44,5	200,1	4497	0,2	2400	43,7
4	43,7	199,4	4563	0,2	2400	45,0
		Average	**4572**		**Average**	**45,2**

The dynamic elastic modulus 45,2 GPa is not used for further calculations, since capacity equations normally consider the secant modulus.

5 Results of experiment

5.1 Strain at prestress

Measured strain in the BFRP tendons over 26 days (Figure 5-1). The measure starts before

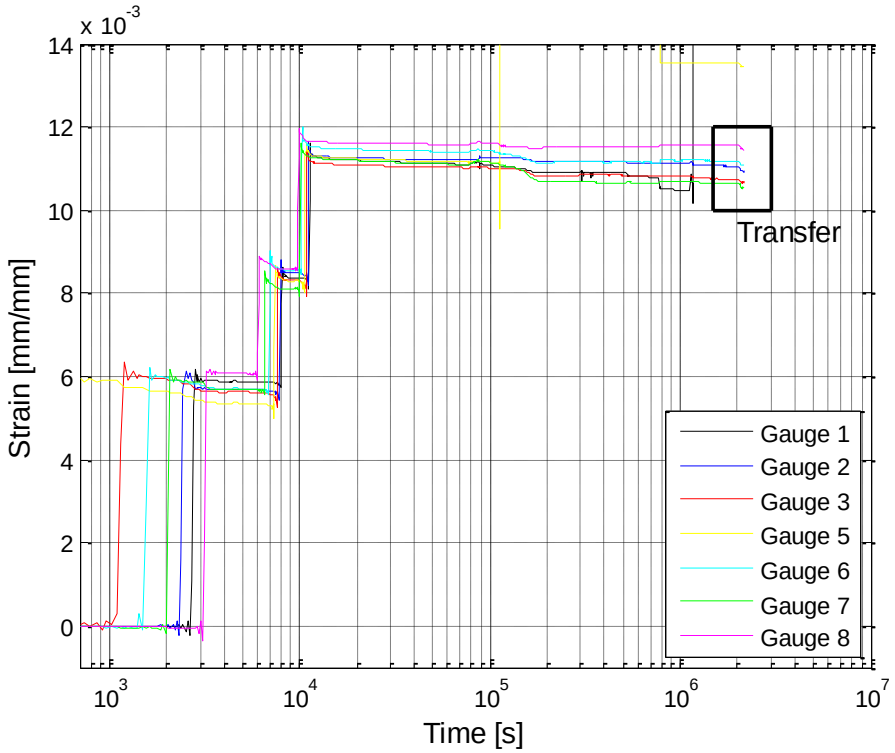

Figure 5-1 Strain in the BFRP tendons. Gauges 1 and 2 represent beam 4, gauges 3 and 4 represent beam 3 and etc.

prestress, and 25 hours before casting. On the time scale casting takes place at 9 x 10^4s and the heat effect of curing in the concrete can be seen in the stress variation for ca. 30 hours after casting, until 2 x 10^5 s. The heat variation in the concrete due to curing and the high humidity disturbs the gauge's measurements in this period. Gauges 2 and 8 retain nearly the same strain after the curing of the concrete, but the strain reduces in all other tendons, especially gauge 7. Gauges 1 and 5 stopped measuring due to some error, probably because of eduction in the gauges or their electrical wiring.

5.2 Strain at transfer

Decrement of tendon's strain at transfer (Figure 5-2). Strain decrease is similar for all tendons

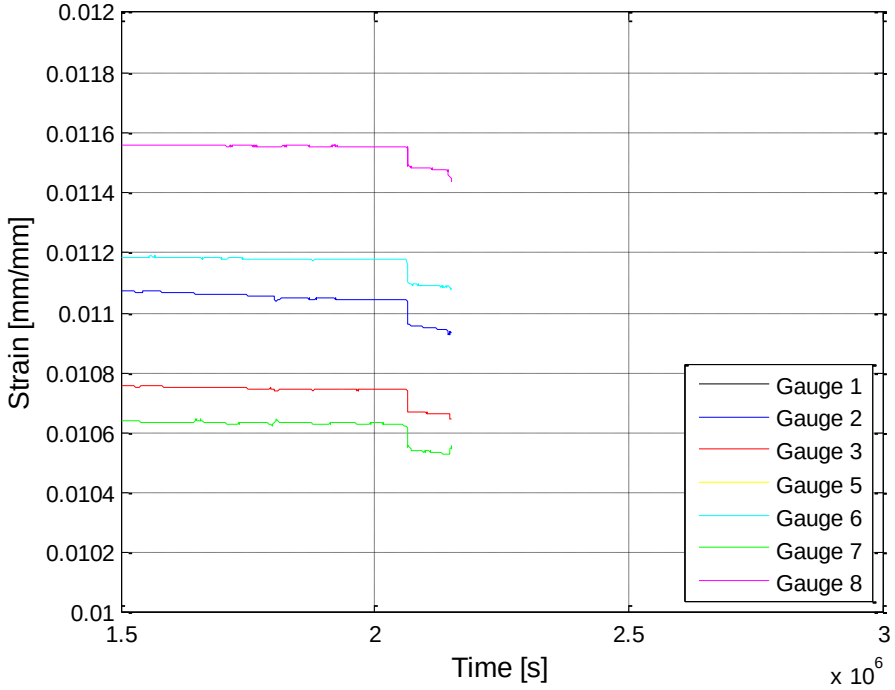

Figure 5-2 Strain at transfer in the BFRP tendons. Gauges 1 and 5 were not functioning properly

0,1‰ for the transfer. Strain measurements were continued for 24 hours after transfer until the beams were taken out of the form work. Variation of strain was less than 1‰ between gauges after transfer, but the largest difference was between gauges 7 and 8 which represent the same beam.

5.3 Estimated effective prestress force

Assuming the BFRPs modulus of elasticity 50 GPa (see appendix A) and prestress of 600 MPa then strain in the tendon would be 12‰ (Figure 5-3). The effective prestress force for each tendon can be calculated according to the strain measurements and Hooke's law (Table 5-1).

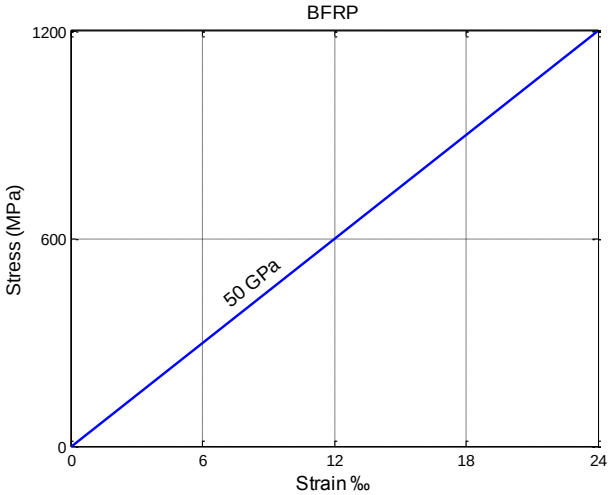

Figure 5-3 Stress strain relationship for the BFRP tendons

$$P_F{}' = E_F * \varepsilon' * A_F \quad \text{(5-1)}$$

$P_F{}'$ is the effective prestress force.

E_F is Young's modules for the BFRP tendons.

ε' is the effective strain in the BFRP tendons after losses.

A_F is cross section area of the BFRP tendons.

Table 5-1 Effective prestress force after losses, ΔP is the lost prestress force

Tendon/gauge no.	Strain mm/mm	P' kN	ΔP kN	Losses %
1	xx	xx	xx	xx
2	0,01093	42,9	4,1	9,5
3	0,01065	41,8	5,2	12,4
4	xx	xx	xx	xx
5	xx	xx	xx	xx
6	0,01140	44,8	2,2	5,0
7	0,01053	41,4	5,6	13,7
8	0,01148	45,1	1,9	4,3
			Mean:	**8,96**

The largest difference is between tendons 7 and 8 which are both located in beam 1. The difference is 3,7 kN, that is 8,9% higher effective prestress force in tendon 8 than tendon 7.

5.4 Discussion

Strain in the BFRP tendons at prestress should be 12‰ due to the prestress force 47 kN (Figure 5-3). Most of the tendons reach that strain at prestress or at least 11,2‰ but lose approximately 0,5‰ strain right after prestressing, or in the first hour (Figure 5-1). Relaxation in the prestress bench could be the reason for this loss or a part of it. Otherwise the tendon relaxation until concrete curing is rather low. Heat from curing of the concrete could have damaged some gauges, and therefore they measure considerably lower strain afterwards. Furthermore some tendons seem to gain strain as time passes which is impossible. Because of uncertainty in the strain measurements and short duration, it isn't sensible to estimate the longtime relaxation of the tendons. It would be more convenient to measure the relaxation on striped tendons, not in concrete beams as was the original plan. Furthermore the measuring period would have to be longer.

5.5 Flexural testing of beams without external shear reinforcement

Beams were numbered in the order that they were taken out of the form work. Therefore, beam 4 was tested first. Gauges 1 and 2 measure the tendon strain.

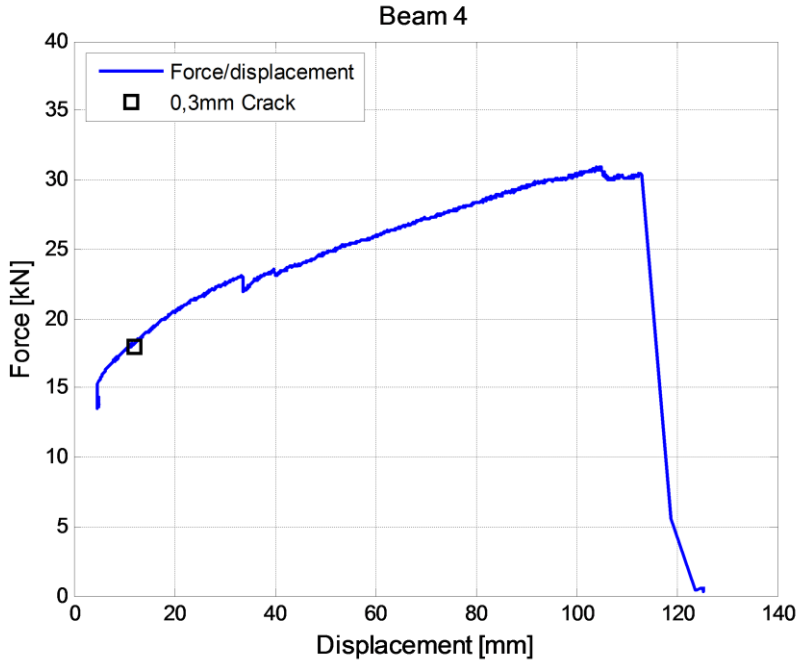

Figure 5-4 Force-displacement relationship for beam 4

The first cracks that were wider than 0,3 mm occurred at 18 kN force. The concrete tension area fails at approximately 23 kN and tendons take over all tension force. The force drops in that instant, as can be seen on the twist in the line (Figure 5-4). Maximum force was 30,9 kN and maximum displacement 117 mm. Maximum strain in tendon 2 was 23,8‰, tension and 3‰ in the concrete, compression (Figure 5-5). The beam failed in shear, although flexural cracks and deflection were significant.

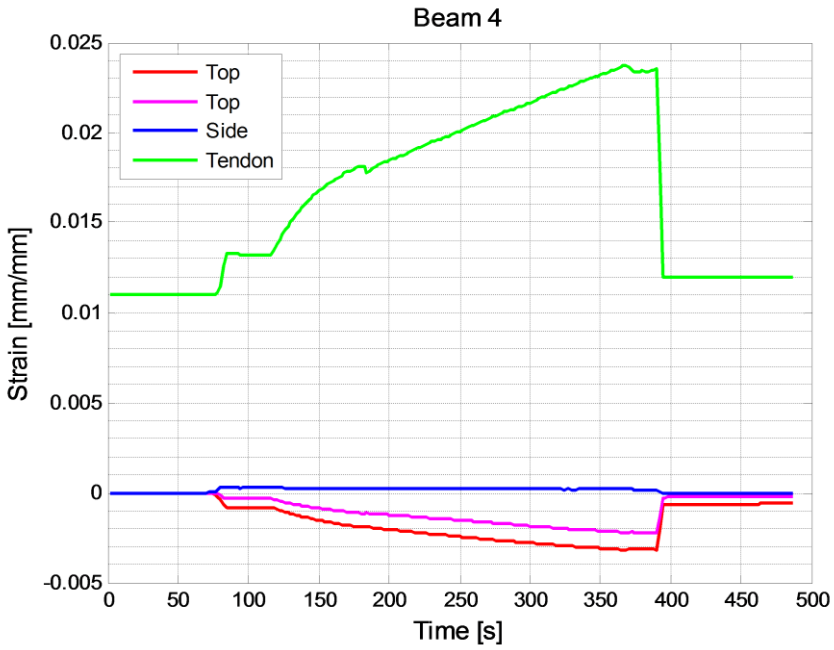

Figure 5-5 Strain at bending, tendon 2 and concrete at extreme fibers

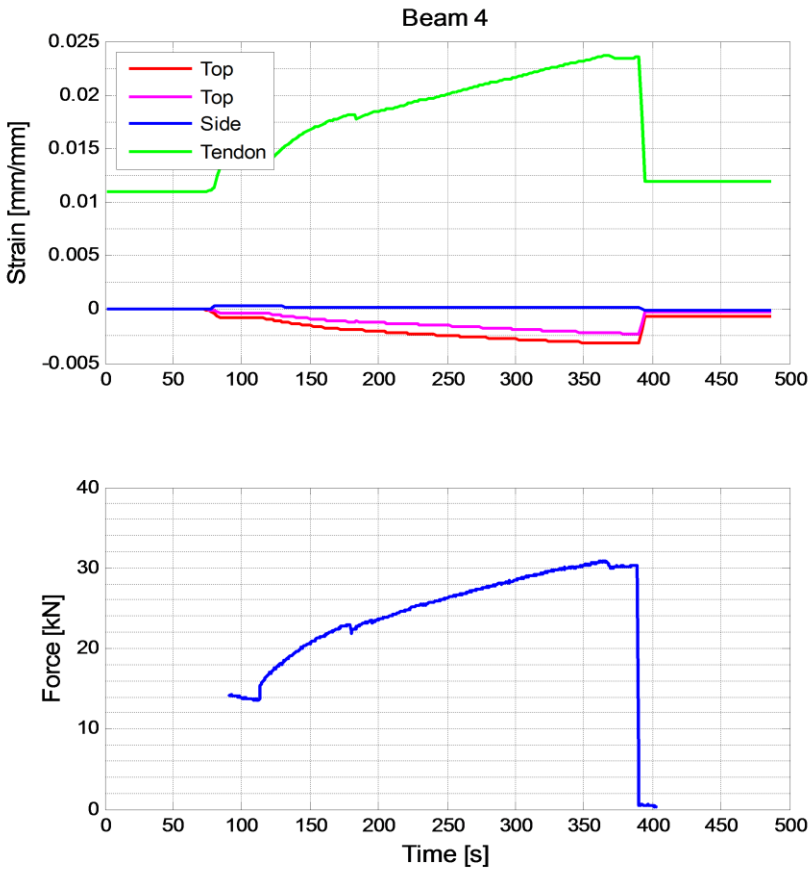

Figure 5-6 (Upper) Strain at bending as a function of time, tendon 2 and concrete at extreme fibers. (Lower) Force as a function of time

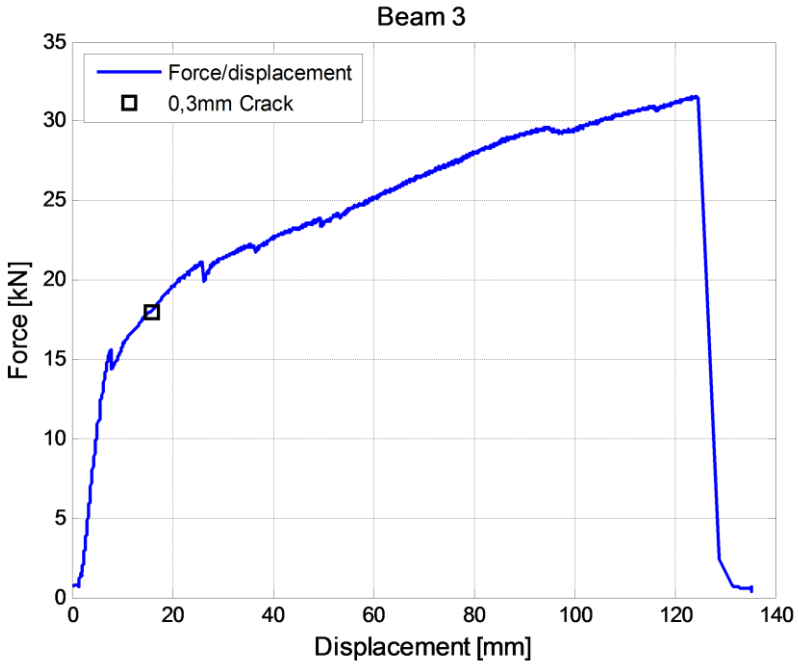

Figure 5-7 Force-displacement relationship for beam 3

First cracks that were wider than 0,3 mm occurred at 18 kN force, but it may have occurred before, at 15 kN force, according to twist in the curve. Concrete tension area fails at approximately 21 kN and tendons take over all tension force. Maximum force was 31,6 kN and maximum displacement 124 mm.

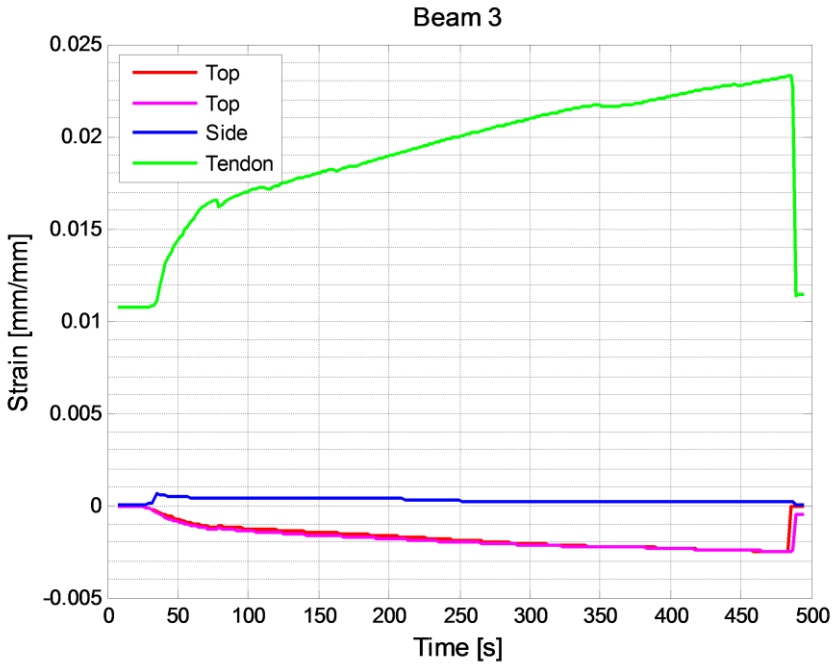

Figure 5-8 Strain at bending, tendon 3 and concrete at extreme fibers

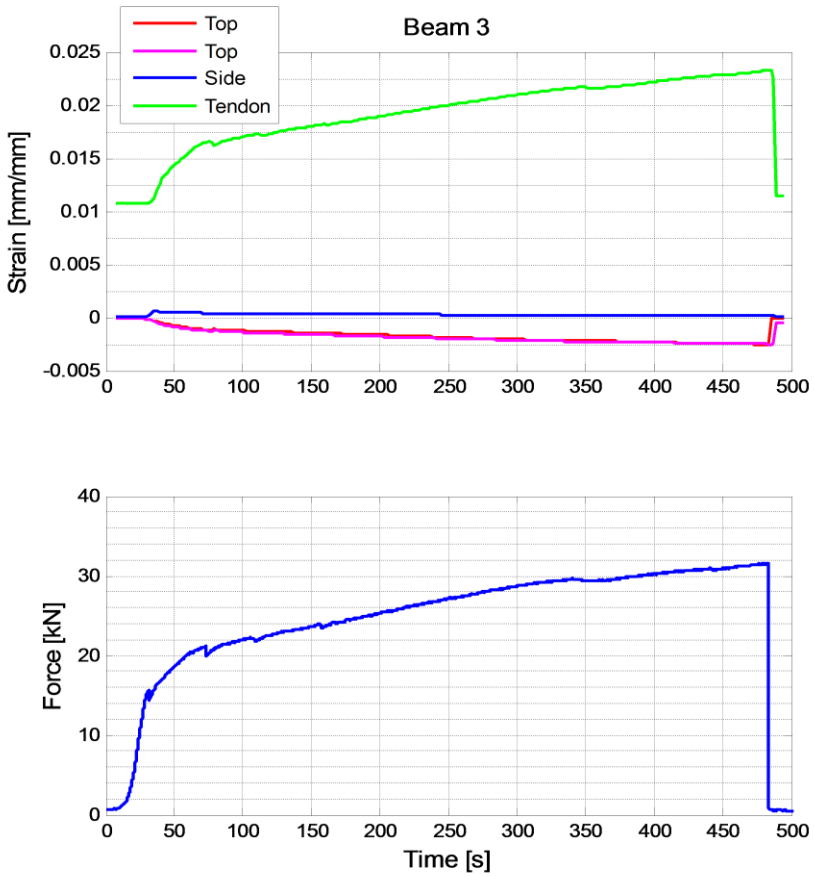

Figure 5-9 (Upper) Strain at bending as a function of time, tendon 3 and concrete at extreme fibers. (Lower) Force as a function of time

Maximum strain in tendon 3 was 23,1‰, tension and 2,5‰ in the concrete, compression. Strain on the beam side was rather low, but in the beginning, it increases with rising force almost until the first cracks occurred (Figure 5-8 and 5-9). Beams 3 and 4 both failed in shear (Figure 5-10 and Figure 5-11).

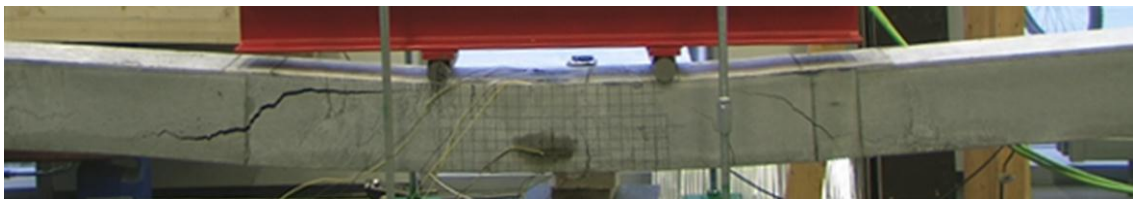

Figure 5-10 Failure mode of beam 4

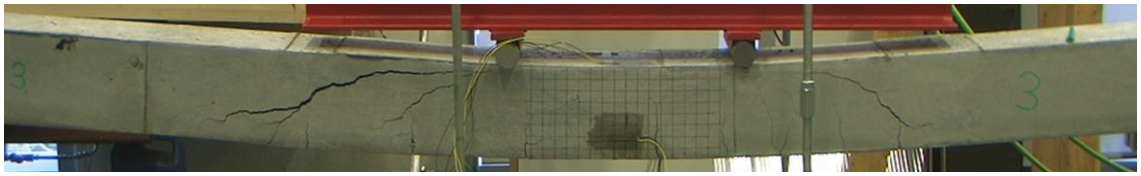

Figure 5-11 Failure mode of beam 3

a)

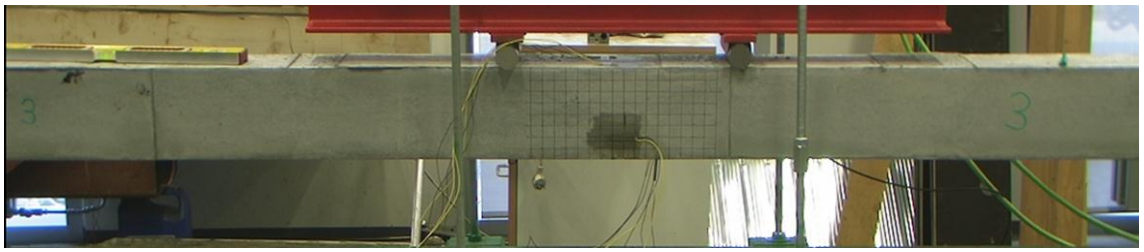

b)

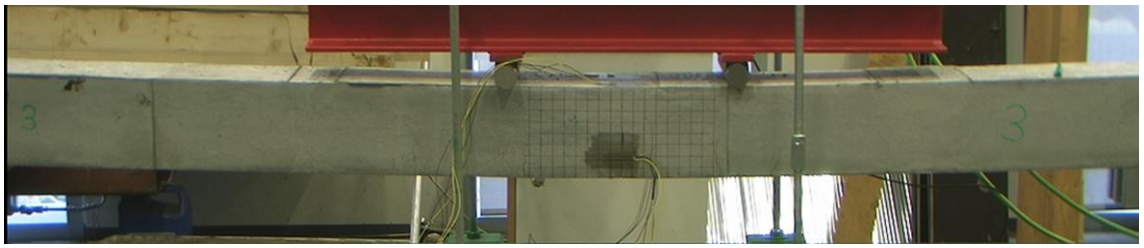

c)

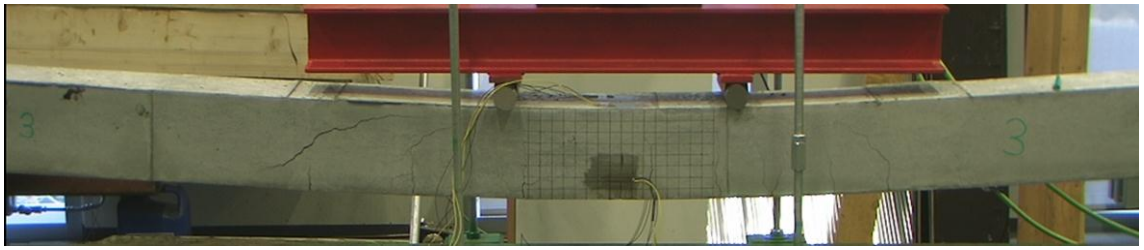

d)

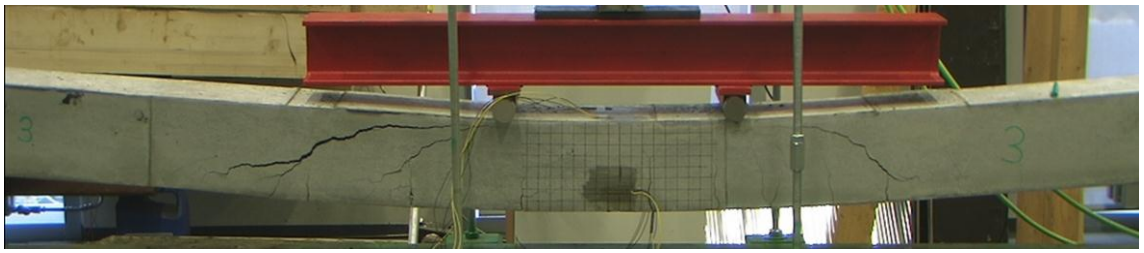

e)

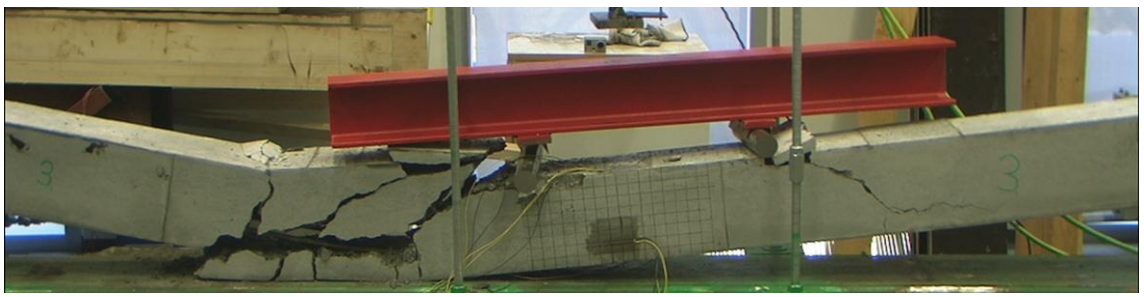

Figure 5-12 a) Beam 3 before loading, b) Beam 3 near service loading c) Beam 3 when diagonal cracks start developing d) Beam 3 near failure e) Beam 3 after failure

Figure 5-12 shows the failure mode for beam 3, which was very similar to beam 4. At the early stage of the specimens increment of deflection and strain were relatively low compared to the incitement of loading. When loading reached 15-18 kN, vertical cracks started to develop from the lower edge of the beam. At this stage both displacement and strain started to rise more rapidly. Further vertical flexural cracks developed, former cracks elongated and widened up as the loading went on. When loading reached 21-23 kN the concrete tension zone failed, force displacement relationship and force strain relationship became almost linear until complete failure. Diagonal cracks developed 350-500 mm from the loading points at loading 24-26 kN, they headed in nearly 45° angle in the direction of the beam. As loading increased these cracks elongated and widened up, much faster than the vertical flexural cracks and were wider. The critical diagonal cracks longed and became nearly horizontal 20 mm from the top and 50 mm from the bottom, which was in level with the tendons. Both beams failed on the left side to the jack (Figure 5-10 and Figure 5-11) although diagonal cracks started on the right side. Right before failure the strain and force increment slacks, but deflection continues especially at beam 4. Maximum load was rather similar for both beams 30,7 kN and 31,6 kN. Tendons didn't fail in either of the beams.

5.6 Discussion

Beams 3 and 4 failed in shear, which was unexpected for beams with such high a/d ratio 10,67. Shear force at failure was 15-16 kN which is nearly 50% lower than former testing showed for the same sections 27-33,5 kN in Jónsson's thesis, 2011. The shear capacity of beams 3 and 4 was similar to the calculated capacity with equation (3-1) 13,7 kN but considerably lower than fib40 (EC2) and fib40 (ACI) equations 18,5 kN and 31,4 kN (Table 3-2). This will be discussed further in chapter 6.

Since the main objective of the experimental work of this thesis was to investigate beam moment capacity, and the beams failed in shear, it was decided to strengthen beam 1 and 2 against shear. Beams 3 and 4 showed very similar results, both the failure modes and ultimate force, therefore there were further testings with un-shear strengthened beams of little addition to the results. External stirrups were fitted to beams 1 and 2 (Figure 5-13), see section 4.10.

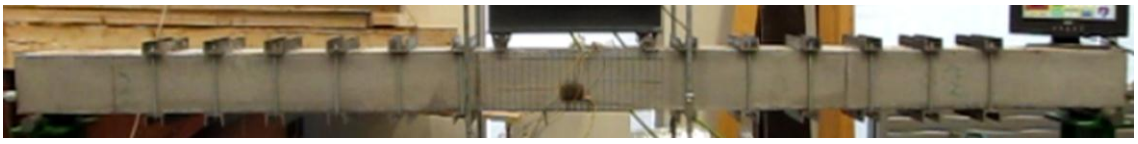

Figure 5-13 External stirrups on beams 1 and 2

5.7 Flexural testing on beam with external shear reinforcement

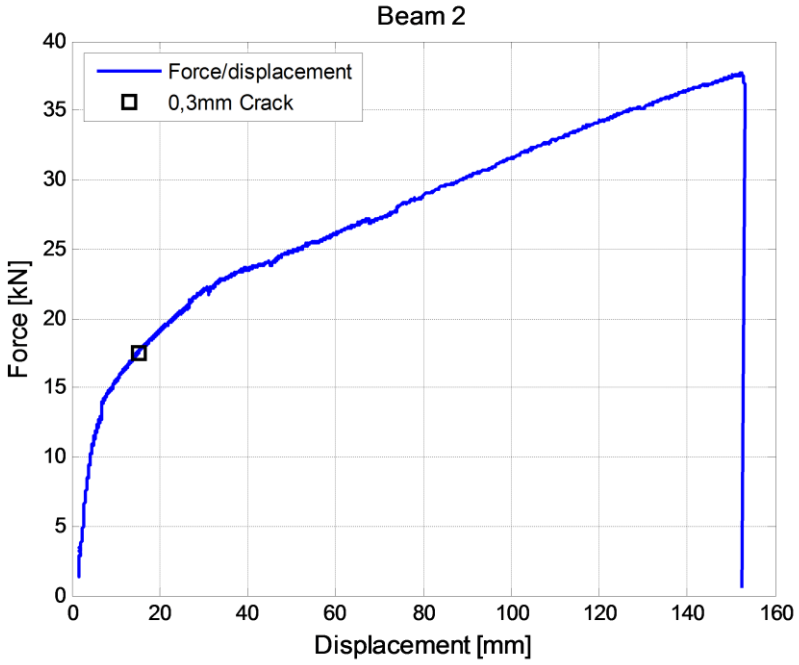

Figure 5-14 Force-displacement relationship for beam 2

First cracks that were wider than 0,3 mm occurred at 17,5 kN force. Concrete tension area fails at approximately 21 kN and tendons take over all tension force. Maximum force was 37,7 kN and maximum displacement 153 mm.

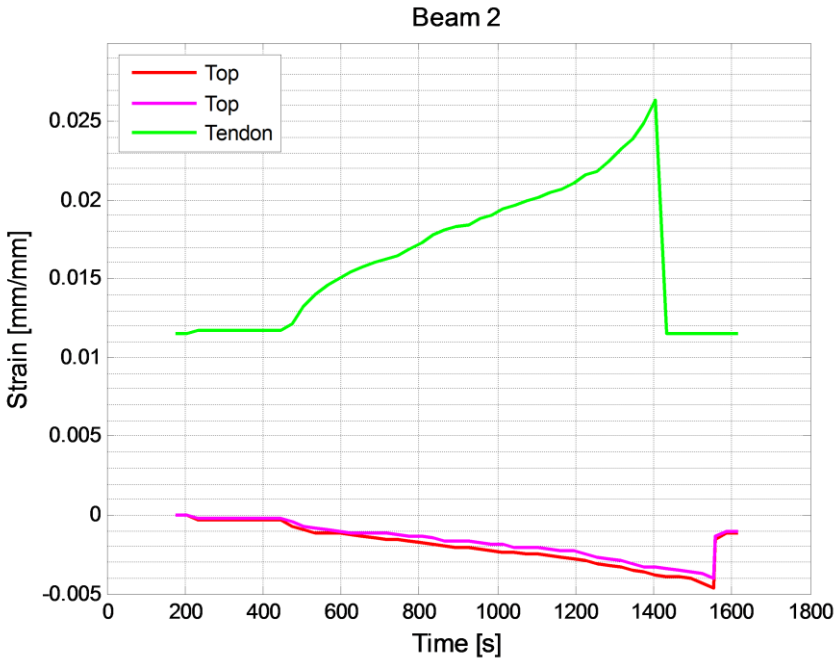

Figure 5-15 Strain at bending, tendon 6 and concrete at extreme fibers

Maximum strain in tendon 6 was 26,4‰ tension, but the gauge was out of bounds and stopped measuring before failure. Maximum strain in the concrete was 4-4,5‰, compression.

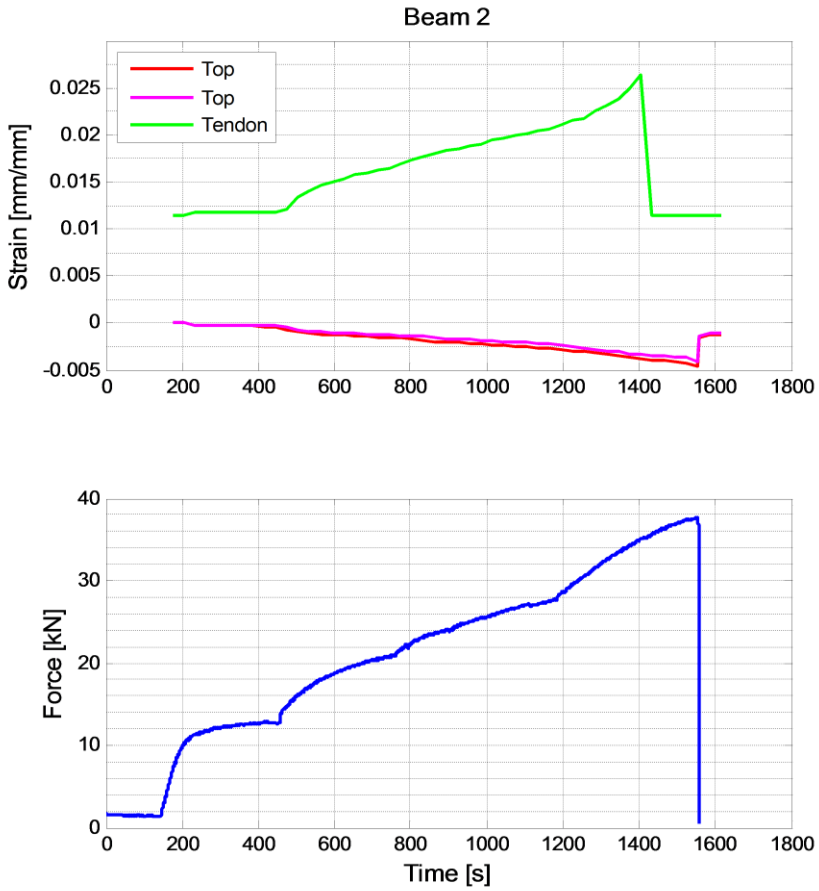

Figure 5-16 Strain at bending as a function of time, tendon 6 and concrete at extreme fibers. (Under) Force as a function of time

Measurements for strain on the site perished (Figure 5-15).

The difference in load increments with time was because of stepping in rotation speed of the hydraulic pump.

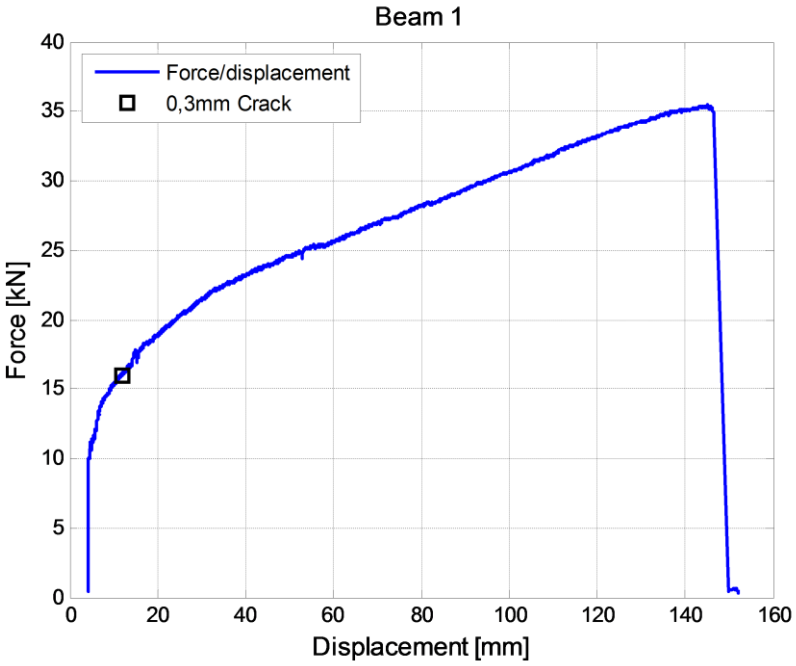

Figure 5-17 Force-displacement relationship for beam 1

First cracks that were wider than 0,3 mm occurred around 16 kN force. Concrete tension area fails at approximately 19 kN and tendons take over all tension force. Maximum force was 35,4 kN and maximum displacement 147 mm. Maximum strain in tendon 7 was 26‰ and 26,1‰ in tendon 8. Both gauges got out of bounds. Maximum strain in the concrete was 4-4,5‰, compression.

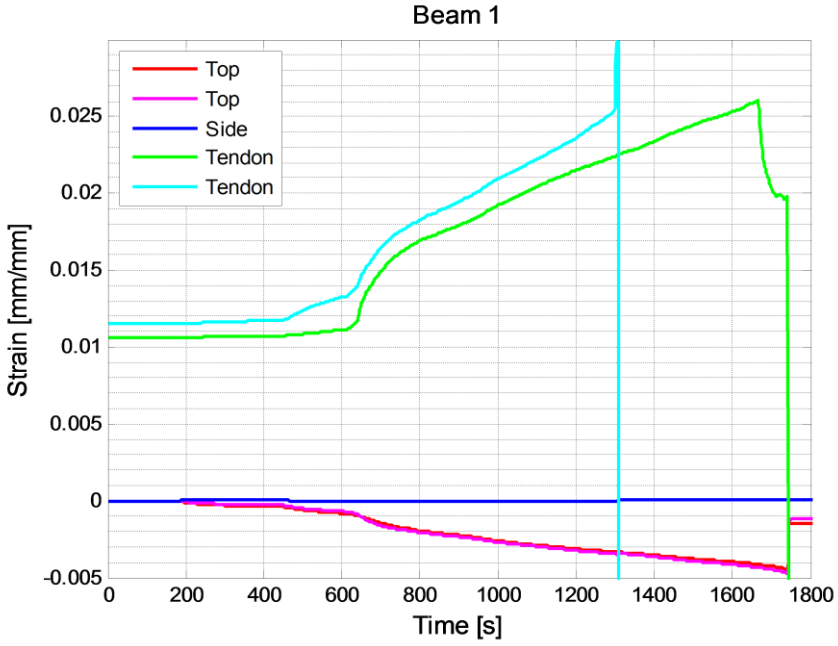

Figure 5-18 Strain at bending, tendon 7 and 8, also concrete at extreme fibers

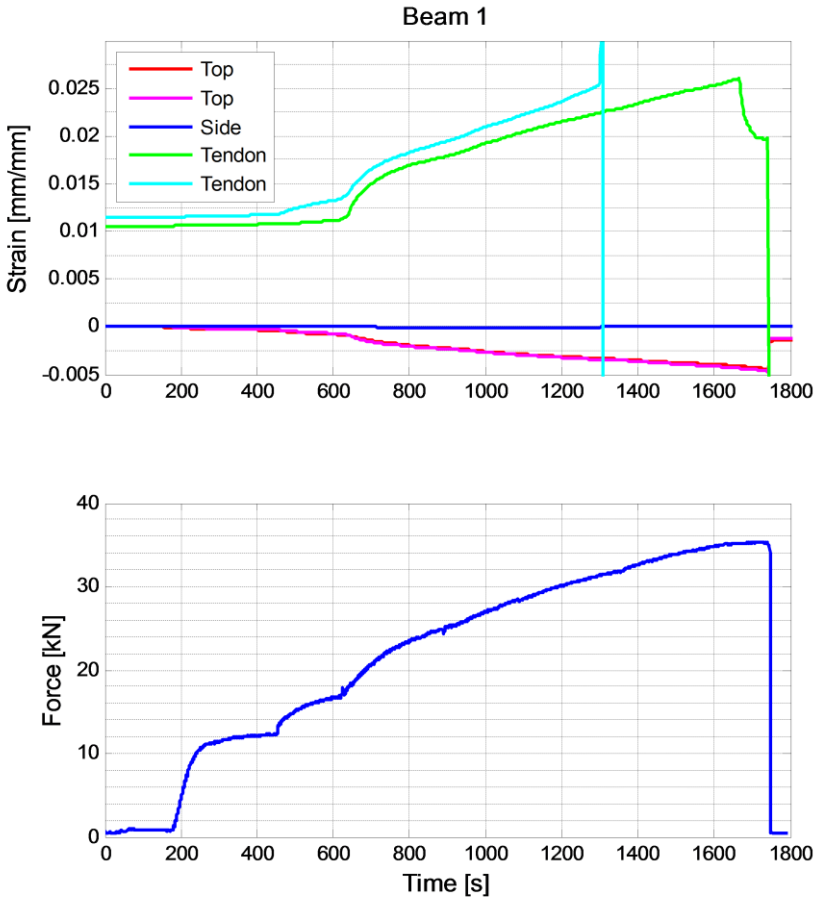

Figure 5-19 Strain at bending as a function of time, tendon 7 and 8, also for concrete at extreme fibers. (Lower) Force as a function of time

Beams 1 and 2 had very similar failure modes, typical bending failures due to tendon rupture (Figure 5-20).

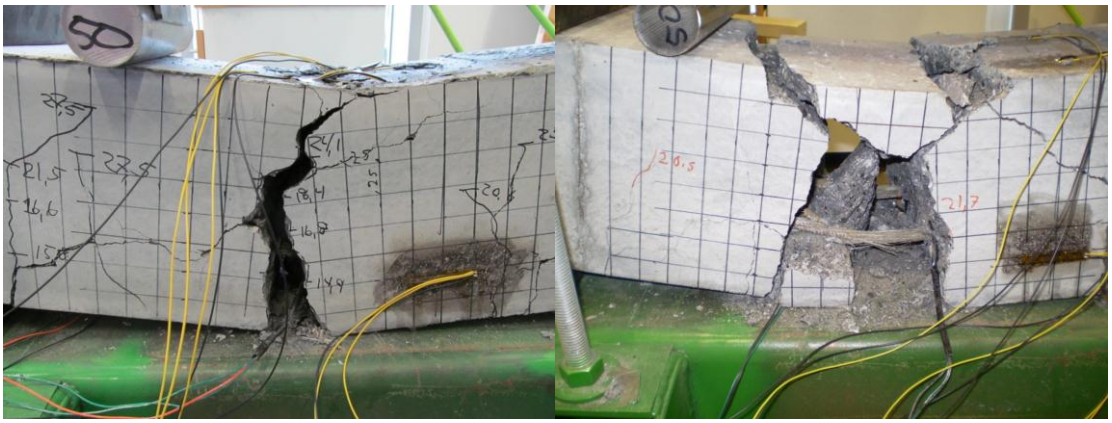

Figure 5-20 (Left) Failure mode of beam 1 (Right) Failure mode of beam 2

a)

b)

c)

d)

e)

Figure 5-21 a) Beam 1 before loading, b) Beam 1 near service loading, flexural cracks have developed c) Beam 1 when flexural cracks have become significant d) Beam 1 near failure e) Beam 1 after failure

Beams 1 and 2 both failed at bending in the middle due to similar force 35,4 kN and 37,7 kN where tendons failed in both cases. Deflection at ultimate loading was also rather similar for both beams 147 mm and 153 mm. (Figure 5-21) shows failure mode for beam 1 which was very similar to beam 2. At the early stage of specimens force, deflection and cracking were

very similar to beam 3 and 4. When loading reached 12-15 kN, vertical cracks started to develop from the lower edge of the beam. Displacement and strain started to rise more rapidly until the concrete tension zone failed around 19-21 kN. Afterwards, the force displacement relationship was nearly linear until complete failure. Diagonal cracks developed in beam 1 between stirrups one and two from the middle. Those cracks got visible around 26 kN force and widened up as the load increased, but did not lead to failure. Further flexural cracks developed, former cracks eloigned and widened up as loading went on. Critical flexural cracks laded up from the lover edge of the beam, up to 50 mm from the top (Figure 5-22). When tendons failed completely, these cracks eliminated to the top, i.e. were neutral almost at the top.

Figure 5-22 Zoomed in on beam 1 right before failure

Strain measurements for tendons of beams 1 and 2 all went out of bounds and stopped measuring around 26‰ strain. Maximum strain in the concrete at the top was 4-4,5‰ in compression for both beams. Strain measurements on the side of the beam didn't show any significant results.

Figure 5-23 (Left) Cracks on top of beam 2 after failure (Right) Beam 1 after failure, seen from end

After failure of beam 2 cracks were noticed on top of the beam, between the stirrups perpendicular to the beam across the top surface (Figure 5-23, left). It is not known for sure whether those cracks developed while testing or after failure, when tendons failed and the beam landed on the testing equipment. After testing when the beam had been broken in half, each part was almost rectilinear (Figure 5-23, right) and while testing, the most curvature was around the mid span of the beam.

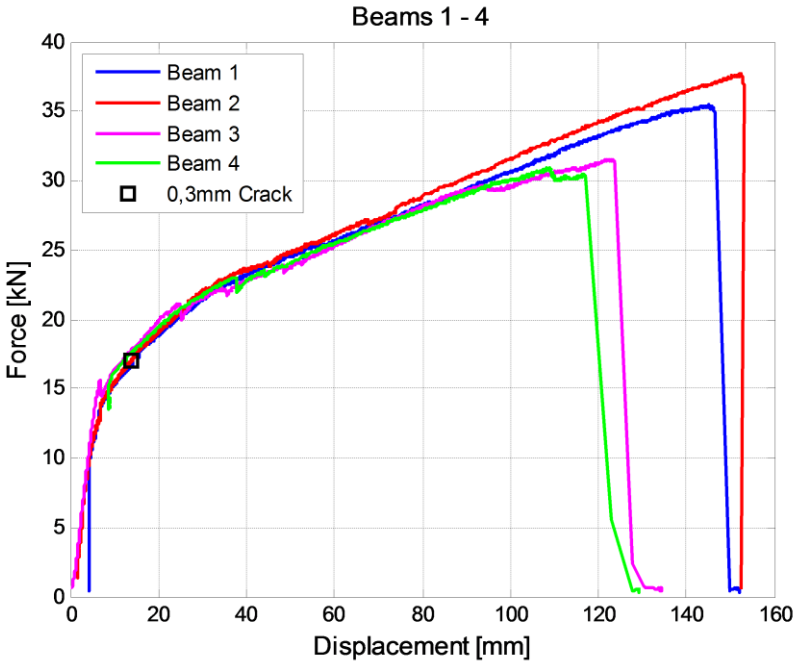

Figure 5-24 Force displacement relationship for beams 1-4

All four beams have very similar force-deflection relationship up to around 30 kN force, when beams without shear strengthening start lacing (Figure 5-24). That is at around the same load as the diagonal shear cracks start to widen up.

5.8 Discussion

Results for both sets of beams are rather similar and comparable. After testing of beams 3 and 4 which both failed in shear, it was decided to shear reinforce the remaining beams. This external shear reinforcement functioned rather well and prevented flexural shear failure although some diagonal or horizontal cracks occurred, but did not lead to failure. Estimating cracks widths was rather subjective and some cracks may have been overlooked, but the measurements should give reasonable results for maximum load at serviceability limit state (SLS). Measuring crack widths gives additional information about the service load ability as

well as the deflection. Displacement was measured at the jack, which gives little less deflection than the center of the beam due to two point loading. The error is especially low when deflection is small but increases with increased displacement. This is discussed further in chapter 6.

6 Discussion

6.1 Failure modes

Beams 3 and 4 failed unexpectedly in shear. As reviewed in the literature chapter BFRP has low elastic modulus and low transverse strength. Therefore, BFRP reinforced members are subjected to more deflection before failure than steel RC members and have less dowel strength (Bank, 2006). The large deflection leads to more and wider cracking of concrete in the section's tension zone as well as higher neutral axis. These issues above, in addition to distribution of bending moment and shear forces, lead to principal tension stresses greater than the concrete can handle. That results in wide inclining cracks that lead to failure (Bhatt, 2011). The shear force of the section is constant over the span from support to point load and bending moment rises from zero at support, to maximum at point load (Figure 2-1). The shear failure occurred where bending moment is high and shear force at maximum which indicates that shear failures don't only depend on shear force, but also on the combination of shear force and bending moments. The prestress force does also come into this, because of a small compression zone of the section, is it subjected to high prestress which could lead to compression failure (shear-compression failure). Although this was not the case in the experiment, both beams shortened after failure (Figure 6-1). Tendons didn't fail and therefore, the broken parts were drawn to each other, and because of critical cracks inclination, the parts overlapped. This leads to more drastic failure and adds both vertical and horizontal cracks. The beams also demerged in the fall after complete failure. The critical shear crack had an angle of 45° to beams direction, sloped towards sections natural axes at top and tendons at the lower edge. That is not unusual for concrete beams, although Jónsson, 2011 experimental

Figure 6-1 (Left) Beam 3 after failure (Right) Beam 4 after failure

beams had critical shear cracks of 20° to beam axis. This difference could be explained by the difference in a/d ratio and types of failure. In his experiment, beams failed more brittle due to almost diagonal shear failure, but theses experimental beams, having double a/d ratio, failed at flexural shear.

Beams 1 and 2 were shear strengthened with external steel stirrups to prevent shear failure. The stirrups functioned rather well and both beams failed at flexure due to rupture of tendons. The failure was rather brittle, although the fiber rupture could be heard right at failure. Force deflection relationship was almost linear after concrete tension zone failed until complete failure. The fully elastic behavior of BFRP reinforced concrete makes it unattractive for structures where seismic loading can be expected because of no ductility. It was seen that BFRP prestressed beams had outstanding deflection capability which takes up energy and makes up for some of the ductility lack. There were no signs of tendons slipping and therefore it is assumed that anchors worked properly as well as tendons sand coating. Tendons strain was measured highest 26‰ when gauges went out of bounds, but when strain vs. timeline were extended to failure, the maximum strain was estimated 27‰. This particular BFRP's ultimate tensile stress was 1200 MPa and because of elastic behavior Hooke's law can be assumed. Therefore the tendons maximum stress is 1350 MPa if its elastic modulus is 50 GPa or 44,4 GPa if maximum stress is taken as 1200 MPa. Since tendon tensile strength wasn't tested directly, this can't be settled for sure. Ultimate tensile strength is usually higher than producers guaranty because guarantied strength is fractile values. This tendon producer "Magma Tech" doesn't illustrate how the ultimate stress is obtained, and it has been reduced from 1200 Mpa to 1000+ MPa recently which makes this technical information rater unreliable (Appendix A), ("RockBar," n.d.).

Strain in concrete at compression went up to 0,0045 at extreme fibers which is considerably higher than Eurocode 2 recommends ε_{cu2} = 0,00273 according to table 3.1 (EN 1992-1-1, 2004). This conservative value is perfectly understandable, considering the varying properties of concrete. Strain measurements at concretes tension zone did not work, strain rose remotely until first tension cracks developed, then dropped back to zero. The maximum strain was therefore hardly measurable. Since concrete has rather poor tension qualities, the main tension movements are up taken by cracking and the strain is nearly zero between the cracks. Otherwise, strain measuring worked well, except for three gauges, which failed, and stopped measuring tendon strain. Measurements agree among themselves and give additional information to this research. It should be kept in mind that a selection of gauges is important,

since they have a limited range of elongation. Furthermore they have to be handled with great care, especially when installed to concrete.

6.2 Comparison of test results and theory

To compare test results and calculations material properties of concrete and fibers used are measured values (section 4.11).

Table 6-1 Measured material properties

Concrete			**Beams 1-2**	**Beams 3-4**
Mean cylinder strength	f_{ck}/f_c	(Mpa)	65,2	57,1
Mean tensile strength	f_{ctm}		4,3	4,0
Elastic modulus	E_{cm}/E_c	(Gpa)	38,6	37,1
Ultimate compressive strain	ε_{cu}		0,004	
BFRP				
Ultimate tensile stress	f_{fu}/f_{pu}	(Mpa)	1200	
Ultimate tensile strain	ε_{pu}		0,026	

The theoretical service load was calculated according to a method addressed in section 3.8, where a combination of stresses from: compression force, tendon eccentric and applied load are set equal to calculated mean tensile strength of concrete.

Theoretical ultimate load was calculated with two ultimate moment capacity methods according to (ACI 440.4R-04, 2004), (ACI) and (EN 1992-1-1, 2004), (EC2) which are addressed in section 3.8. Measured material properties of beams 1 and 2 were used for those calculations since they failed at flexure. As both concrete compressive strain and BFRP's tendons tension strain were measured greater than expected, the theoretical section changed from compression controlled to tension controlled section. Calculations were updated according to these results and can be seen in appendix F.

For comparison of displacement the Icelandic building regulation was considered, where maximum displacement for beams is limited to L/400 or 15 mm for combination of dead and live load. For these beams with span of 3200 mm, a maximum allowed displacement is 8,0 mm.

Tested service load was measured when 0,3 mm cracks occurred in the section and corresponding displacement was measured. Ultimate load was measured at failure with corresponding displacement (Table 6-2).

Table 6-2 Test results, force and displacement

	Test, force (kN)		Theory, force (kN)			Test, displacement (mm)		L/400
	SLS	ULS	SLS	ULS (EC2)	ULS (ACI)	SLS	ULS	(mm)
Beam 1	16	35,4	15	36,6	33,3	12	147	8,0
Beam 2	17,5	37,7				15	153	
Beam 3	18	31,6*	14,5			15	124	
Beam 4	18	30,9*				15	117	

Note: * Shear failure

Tested service load was around 12% higher than expected for beams 1 and 2, but 29% higher for beams 3 and 4. Although this is relatively high difference, it is of the same order as measurement tolerance, keeping in mind that service load measurements were rater subjective. Beams 3 and 4 have slightly higher service resistance than beams 1 and 2, contrary to the calculations, this could be explained by random behavior of concrete cracking.

The mean tested ultimate moment capacity of beams 1 and 2 was almost the same as calculated with the EC2 method, and 10% higher than the ACI method. This indicates that usual methods can be used to evaluate moment capacity of BFRP prestressed concrete. These calculations are strongly depending on the prestress losses, like all prestressed sections. Losses were taken as 20% not 25% because of the young age of the concrete.

Displacement was not a subject of this thesis and therefore not calculated. Measured displacement due to service loading was higher than allowed for all specimens, and therefore displacement limit is dominant for service loading. Force which induces 8 mm displacement is listed in (Table 6-3).

Table 6-3 Service load at limit displacement

	Test force at disp.	
	(kN)	(mm)
Beam 1	14,4	8,0
Beam 2	14,6	
Beam 3	15,0	
Beam 4	14,4	
Mean:	**14,6**	

The mean value 14,6 kN can be taken as mean service load capacity of the beams, where L/400 displacement limit applies. It is desirable to have displacements as a limiting factor of design to prevent concrete cracking, which is undesirable as discussed before.

Back to test result in Table 6-2 where mean ultimate shear strength of beams 3 and 4 is 15,6 kN. Calculated shear strength of the section varies a lot depending on which calculation method is used, which makes these equations rater unreliable (Table 3-2). The strength of this experiment is compared to earlier results of the experiments of Jónsson, 2011 where the mean shear strength was 30 kN (Table 6-4), which is nearly double for the same cross section. The shear span of his specimen beams was 795 mm compared to 1600 mm in this experiment. This indicates again that shear span to depth ratio is important for the shear strength, as stated before.

Table 6-4 Test results for beams in former experiment (Jónsson, 2011, p. 41)

	Test force F (kN).		**F/2 (kN)**
	SLS	**ULS**	**ULS**
Beam 1	33	59,0	29,5
Beam 2	35	67,0	33,5
Beam 3	33,0	54,0	27,0
Mean:	**33,7**	60,0	**30,0**

Most shear equations don't consider the a/d ratio except for equation (3-1) which gives 13,2 kN shear strength for this experiment and 16,4 kN for the former experiment.

$$V_{cf} = 2{,}1\,(\frac{f_c \rho_{fl} d}{a}\frac{E_{fl}}{E_s})^{0{,}3} b_w d \qquad for\,\frac{a}{d} > 2{,}5 \qquad \textbf{(3-1)}$$

Detailed explanations of this equation are listed in section 3.7.

This equation is a little conservative in case of these experiments and even more so in the former experiment. In both cases the beams failed unexpectedly in shear, but more brittle in the former case. Beams can be considered slender in both cases, with a/d ratio over 2,5 which makes it interesting to find out how large the a/d ratio has to be, so this particular cross-section fails at flexure, without stirrups. To estimate the failure mode, shear force and bending moment capacity were plotted against the a/d ratio (Figure 6-2).

Test results from both experiments are used, both shear and moment failures. Moment capacity is calculated according to formerly described EC2 method (section 3.8) and shear

capacity according to equation (3-1). Material properties were according to testing results (Table 4-3) and cylinder strength was set for 60 MPa. Tested, shear and moment are mean failure forces (F/2).

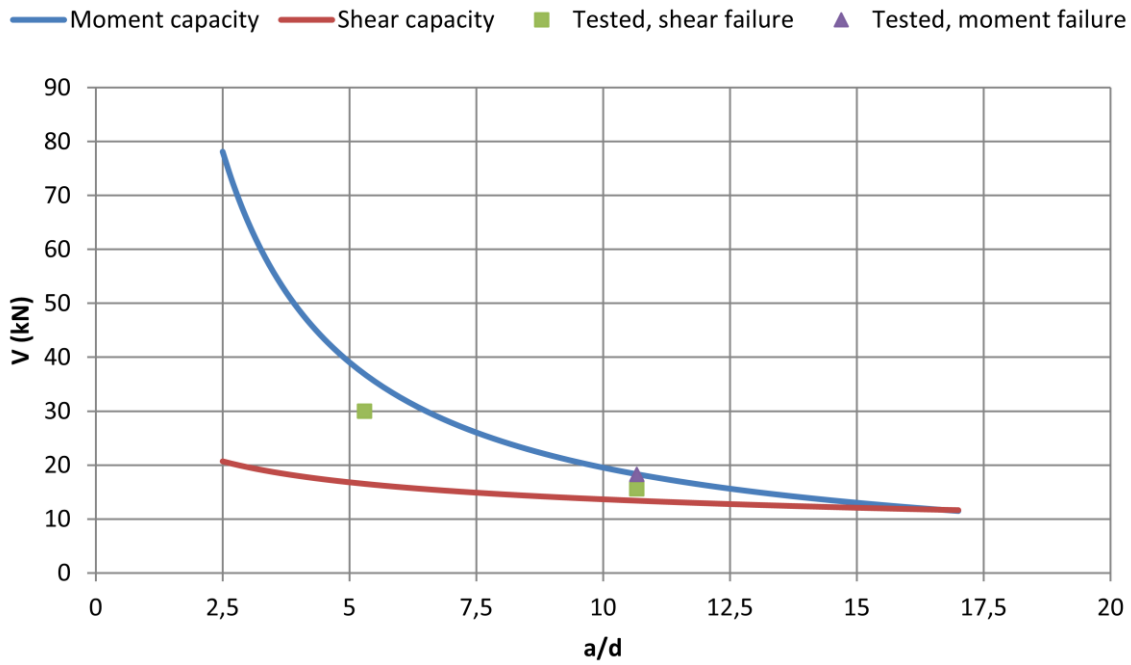

Figure 6-2 Shear force-a/d relationship

Note that this relationship only works for this particular cross section with these specific material properties and is based only on two experiments (seven beam specimens).

Beams with a/d ratio up to 16,6 fail at shear, but more slender beams fail at flexure according to this approach. Considering these results, it is nearly impossible to get flexural failure with this cross section, without shear reinforcement. It is interesting that shear capacity drops about 50% between experiments while the a/d ratio rises by 100%, which means that all beams failed due to the same bending moment. In both cases the ultimate load capacity of the beams would rise about 16% if shear failure were prevented.

Although equation (3-1) considers shear span which is one way to take shear and moment distribution into account it is rather a limited way since loading is always uniform. Another disadvantage is that prestress is not considered although it increases shear capacity.

Shear strength of reinforced and prestressed concrete is debated and partly solved with empirical equations. Many researches have been carried out for steel RC but BFRP is a rather

new material to structural design and therefore, further studies and experiments are recommended to investigate shear behavior.

6.3 Answers to research questions

The main questions for this thesis, asked at the beginning were the following:

- How much is the relaxation of BRFP tendons over a specific time?

  Testing of BFRP relaxation failed and therefore no conclusion can be drawn in that matter. After reviewing relevant literature it can be concluded that more research is needed to estimate long time behavior of BFRP.

- Do load capacity calculation methods, addressed in relevant codes and guides, agree with the experiment?

  Ultimate flexural capacity of the section according to (ACI 440.4R-04, 2004) standard and (EN 1992-1-1, 2004) standard showed very good agreement to flexural test results. The EC2 method which is suited for concrete prestressed with steel, gave exactly the same results as tested and the ACI method which is suited for concrete prestressed with FRP was a little bit conservative, but fully qualified.
  Shear capacity equations gave varying results and need to be considered carefully. Usually shear equations don't consider shear force and bending moment distribution, which has great influence on the shear behavior. Design codes are a bit lacking in this field i.e. FRP prestressed concrete and especially for BFRP.

- What does this and former experiments reveal, regarding BFRP prestressed concrete?

  The experiments showed that BFRP prestressed concrete beams which are subjected to transvers loading, are vulnerable to shear failure. Although beams are slender, with a/d ratio of 5,3 and 10,67 they still fail in shear. Therefore shear capacity needs to be determined with wariness. These experiments and calculations showed that moment capacity was 17% higher than shear capacity and that BFRP can be used to prestress concrete, although its abilities are limited.

- Is BFRP suitable to prestress concrete sections?

  BFRP has some good abilities to prestress concrete sections i.e. high tension strength parallel to fibers, high strength to weight ratio, high rupture strain and corrosion resistance which are the main advantages compared to steel. Since basalt fibers are made nearly entirely from basalt rock, it could become compatible in price to other fibers and maybe sometime steel, which price has been rising rapidly for the past years. The fiber's light weight makes handling easier and reduces transportation cost, which has also been rising due to oil prices.

  The main disadvantages of BFRP are: low modulus of elasticity, low transfer strength, brittle failure, it can't be bent or welded and lack of knowledge about its longtime behavior. To utilize BFRP's high tensile strength it is necessary to prestress it, because of its low elastic modulus, and since tendons can't be claimed or welded, anchoring is a problem. The brittle failure of BFRP is partly solved with over reinforced section which is uneconomical. Its longtime loading abilities are reduced, due to relaxation.

  These mechanical properties make BFRP not all that attractive for structural design. But with more studies, understanding of its functioning, development of resin and relatively lower price, it could become a more desirable choice.

6.4 Recommendations of further research

While working on this experiment and reviewing literature, some questions have been raised and ideas have come up for further researches. Following are a few suggestions for research topics.

- Investigate the longtime behavior of prestressed BFRP tendons and loss of prestress force.
- Perform standard alkali test for the particular BFRP tendons.
- Investigate tendon strength and behavior under thermal conditions.
- Further investigation of anchors for BFRP tendons, used in this research.
- Investigate bond strength between tendons and concrete to estimate transfer lengths.
- Further research regarding the shear capacity of BFRP prestressed beams without shear reinforcement. Investigate varying a/d ratios to establish a new flexural shear formula.

7 Conclusions

Four normal strength concrete beams, prestressed with BFRP tendons were tested under two point loading. The prestressed tendons were anchored with chemical anchors, designed for stressing BFRP tendons, developed at Reykjavik University and modified specially for this experiment (section 4.3).

Two of the specimen beams failed unexpectedly in shear, even with shear span to depth (a/d) ratio of 10,67. The other two beams were shear strengthened with external steel stirrups, which worked properly and beams failed at flexure due to tendon rupture.

Test results were compared to capacity calculations from relevant American and European designing codes and others. Comparison showed that (ACI 440.4R-04, 2004) guide for FRP prestressed concrete and (EN 1992-1-1, 2004) designing code for steel reinforced and prestressed concrete agreed rather well with the test results for flexural capacity.

Several shear capacity equations were reviewed, which gave shear capacity from 20% of tested capacity to 200%.

Test results were compared to recent identical experiments carried out by Jónsson, 2011, on beams with a/d ratio of 5,3. Those beams failed all three unexpectedly in shear, due to double shear force compared to this experiments beams. This indicates that a/d ratio has great effect on the shear capacity although most shear equations don't consider it directly.

BFRP prestressed beams without shear reinforcement are vulnerable to transvers loading even if the a/d ratio is high. Comparison of these experiment results and relevant shear equations showed, that shear force and bending moment distribution along the span or the slenderness of the beams needs to be considered to determinate shear capacity with accuracy and safety.

8 Bibliography

ACI 440.1R-03. (2003). *Guide for the design and construction of concrete reinforced with FRP bars*. ACI Committee 440.

ACI 440.4R-04. (2004). *Prestressing concrete structures with FRP tendons*. ACI Committee 440.

Arya, C., Clarke, J. L., Kay, E. A., & O'Regan, P. D. (2002). TR 55: Design guidance for strengthening concrete structures using fiber composite materials: a review. *Concrete Society*, *24*(7), 889–900. doi:10.1016/S0141-0296(02)00027-5

Ágústsdóttir, E. L., & Sveinsdóttir, S. L. (2010). *Prófanir á basalt trefjastöngum og basaltrefjamottum* (Lokaverkefni í byggingartæknifræði BSc). Reykjavik University, Reykjavik.

Banibayat, P. (2011). *Experimental Investigation of the Mechanical and Creep Rupture Properties of Basalt Fiber Reinforced Polymer (BFRP) Bars* (Doctoral dissertation). University of Akron. Retrieved from http://etd.ohiolink.edu/view.cgi?acc_num=akron1323229543

Bank, L. C. (2006). *Composites for Construction: Structural Design with FRP Materials*. Hoboken, NJ: Wiley.

Bhatt, P. (2011). *Prestressed concrete design to Eurocodes*. London: Spon.

Broddason, Þ. (2012, February 17). *Basalttrefjar*. Presented at the Steinsteypudagurinn, Grand hotel Reykjavik.

CNR-DT 203. (2006). *Guide for the design and construction of concrete structures reinforced with fiber-reinforced polymer bars*. Rome: CNR-Advisory committee on technical recommendations for construction.

De Lorenzis, L., & Teng, J. G. (2007). Near-surface mounted FRP reinforcement: An emerging technique for strengthening structures. *Composites Part B: Engineering, 38*(2), 119–143. doi:10.1016/j.compositesb.2006.08.003

EN 1992-1-1. (2004). *Eurocode 2 - Design of Concrete Structures, Part 1 - 6: General Rules and Rules for Buildings*. European Prestandard: European Committee for Standardization.

FRP reinforcement in RC structures. (2007).fib Bulletin No. 40. Lausanne. Switzerland: International Federation for structural concrete (fib). Retrieved from http://www.fib-international.org/frp-reinforcement-in-rc-structures

GangaRao, H. V. S., Taly, N., & Vijay, P. V. (2007). *Reinforced concrete design with FRP composites*. Boca Raton, Fla: CRC Press.

Hylse med indv gevind HIS-N M12X125: Varenr.: 00258017. (n.d.). Retrieved February 27, 2012, from http://www.hilti.dk/holdk/page/module/product/prca_productdetail.jsf?lang=da&nodeId=-222859&selProdOid=257847

ISIS Education Committee. (2007). *ISIS Educational Module 9: Prestressing concrete structures with fibre reinforced polymers*. Calgary: Department of Civil Engineering, University of Calgary.

Jónsson, B. S. (2011). *Prestressed BFRP tendons in concrete beams*. Master's thesis: Reykjavik University, Reykjavík. Retrieved from http://skemman.is/item/view/1946/9905

Kiekens, P., Van de Velde, K., & Van Langenhove, L. (2003). *Basalt fibres as reinforcement for composites*. Zwijnaarde, Belgium: Department of Textiles, Ghent University. Retrieved from http://www.basaltex.com/files/cms1/basalt-fibres-as-reinforcement-for-composites_ugent.pdf

Klæbemørtel HIT-RE 500/330/1: Varenr.: 00305074. (n.d.). Retrieved March 1, 2012, from http://www.hilti.dk/holdk/page/module/product/prca_productdetail.jsf?lang=da&nodeId=-222850&selProdOid=225544

Li, H., Xion, G., Xiao, B., & Wu, J. (2010). Comprehensive characterization of BFRP applied civil engineering (pp. 65–68). Presented at the *The 5th International Conference on FRP composites in civil engineering*, Beijing,China: School of Civil Engineering, Harbin Institute of Technology, Harbin, China.

McCormac, J. C., & Brown, R. H. (2009). *Design of Reinforced Concrete* (8th ed.). Hoboken, NJ: Wiley.

Nehdi, M., El Chabib, H., & Saïd, A. A. (2007). Proposed Shear Design Equations for FRP-Reinforced Concrete Beams Based on Genetic Algorithms Approach. *Journal of Materials in Civil Engineering*, *19*(12), 1033–1042. doi:10.1061/(ASCE)0899-1561(2007)19:12(1033)

Nordin, H., & Täljsten, B. (2006). Concrete Beams Strengthened with Prestressed Near Surface Mounted CFRP. *Journal of Composites for Construction*, *10*(1), 60–68. doi:10.1061/(ASCE)1090-0268(2006)10:1(60)

Novitskii, A. G., & Efremov, M. V. (2011). Some aspects of the manufacturing process for obtaining continuous basalt fiber. *Glass and Ceramics*, *67*(11-12), 361–365. doi:10.1007/s10717-011-9299-7

O'Brien, E. J., Dixon, A. S., & Sheils, E. (2012). *Reinforced and prestressed concrete design: The tomplete process* (2nd ed.). Edinburg: Spon.

Okelo, R., & Yuan, R. L. (2005). Bond Strength of Fiber Reinforced Polymer Rebars in Normal Strength Concrete. *Journal of Composites for Construction*, *9*(3), 203–213. doi:10.1061/(ASCE)1090-0268(2005)9:3(203)

Ramadass, S., & Thomas, J. (2010). Flexure-shear analysis of concrete beam reinforced with GFRP bars. Presented at the *The 5th International Conference on FRP Composites in Civil Engineering*, Beijing, China: Civil Engineering Division, School of Engineering, Cochin University of Science and Technology, Cochin, Kerala, India.

Ramakrishnan, V., & Panchalan, R. K. (2005). A New Construction Material—Non-Corrosive Basalt Bar Reinforced Concrete. In V. M. Malhotra & P. R. Lago Helene (Eds.), *Quality of concrete structures and recent advances in concrete materials and testing: an international conference honoring V. Mohan Malhotra* (Vol. 229, pp. 253–270). Michigan, IL: American Concrete Institute.

RockBar: Corrosion resistant basalt fibre reinforcing bars. (n.d.). Retrieved from http://magmatech.co.uk/downloads/ROCKBAR_4P.pdf

Sharbatdar, M. K., & Saatcioglu, M. (2009). Seismic design of FRP reinforced concrete structures. *Asian Journal of Applied Sciences*, *2*(3), 211–222. doi:10.3923/ajaps.2009.211.222

Sumida, A., & Mutsuyoshi, H. (2008). Mechanical Properties of Newly Developed Heat-Resistant FRP Bars. *Journal of Advanced Concrete Technology*, *6*(1), 157–170. doi:10.3151/jact.6.157

W.H, M., Bungey, J., & Hulse, R. (2007). *Reinforced Concrete Design* (6Rev Ed.). Palgave Macmillan.

Waldon, P. (2005). The use of FRP as embedded reinforcement in conccrete. In R. Seracino (Ed.), *FRP Composites in Civil Engineering - CICE 2004*. London. UK: A.A Balkema Publishers, Leiden, The Netherlands.

Wu, J., Li, H., & Xian, G. (2010). Influence of Elevated Temperature on the Mechanical and Thermal Performance of BFRP Rebar. Presented at the *CICE 2010 - The 5th International Conference on FRP Composites in Civil Engineering*, Beijing, China:

School of Civil Engineering, Harbin Institute of Technology, Harbin, China. Retrieved from http://www.iifc-hq.org/proceedings/CICE_2010/for+pub/Vol%20I/02%20Materials%20and%20Sustainability/091%20Influence%20Xian.pdf

Xiao, B., Li, H., & Xian, G. (2010). Hygrothermal Ageing of Basalt Fiber Reinforced Epoxy Composites. Presented at the *The 5th International Conference on FRP Composites in Civil Engineering*, Beijing, China. Retrieved from http://www.iifc-hq.org/proceedings/CICE_2010/for+pub/Vol%20I/07%20Long-Term%20Performance/093%20Hygrothermal%20Xian.pdf

Zsutty, T. C. (1971). Shear strength predictions for separate categories of simple beam tests. *ACI Journal, Proceedings*, *68*(2).

9 Appendixes

A. Rock bars

Information about the Rock bars from the manufacturer, Magma Tech

RockBar

Corrosion resistant basalt fibre reinforcing bars

RockBar is a range of basalt fibre composite reinforcing bars for use in Concrete, Mortar and Cast Stone

The properties of **RockBar** include:

- Excellent chemical and corrosion resistance
- 3.7 times lighter than steel and stainless steel
- 2.5 times stronger in tensile strength than steel and stainless steel
- Over 60 times less thermally conductive than steel and over 20 times less thermally conductive than stainless steel
- Non magnetic
- Electrically non-conductive

Environmental performance of **RockBar** includes:

- 40% lower global warming impact than stainless steel
- No waste production during manufacture
- Basalt is one of the most common rock types in the Earth's crust

RockBar technical information

Length	Stock lengths are 2.5m. Cutting to required lengths is possible.
Nominal Diameters	3mm, 4mm, 5mm, 6mm, 7mm, 8mm, 10mm, 12mm, 16mm, 20mm Other diameters available on request.
Composition	Basalt fibre reinforced polymer (BFRP) bar with a sanded finish to aid bonding to mortar.
Tensile strength	1000 Mpa +
Elastic Modulus	50 Gpa +
Bond Strength	10 – 30% higher bond strength than ribbed stainless steel rebar in pull out tests from Cast Stone.
Durability	Durability tests which model the alkali environment of concrete have been completed at Sheffield University The report concludes that; "The estimated environmental strength reduction factor for a period of 100 years wet concrete conditions is 1.25 which corresponds to a strength retention of 79.6 %".
Sustainability	A life cycle analysis has been conducted at Imperial College London. The report concludes that; "The production of stainless steel bars emits ~170% more CO2 than the BFRP bars".
Coefficient of Thermal Expansion	2 x 10-6 1/k (in the longitudinal direction)
Thermal Conductivity	0.7 W/K.m

MagmaTech

www.magmatech.co.uk
contact: Ben Williams
Tel: +44(0)7916155822
Fax: +44(0)8701236392
ben.williams@magmatech.co.uk
PO Box 59162 • London • NW2 9HD

B. Concrete mixture details

Concrete mixture details from the manufacturer BM Vallá.

framleiðslu kýrsla

23.febrśar 2012

afhending nr.: **68183** **Á leið** **gerandi:** Plant manager

hleðslutími 10:20 23.2.2012 **bið um hleðslu framleitt:** 2,00 m³ 2,00 m³ **endursent ma** **heildarmagn: afhent:** 2,00 m³ 2,00 m³ **brottför.: raunv.:** 10:21 10:21 **koma:** 10:41 **hleðslutími:** 11:11 **endursenda** 11:11 **til baka:** 11:31

seljandi: 0 --- **viðskiptav** 3804 Háskólinn í Reykjavík ehf Ofanleiti 2 **103** **vinnustaður:** 29123 Háskólin reykjavíkur

aths.:

verksmiðja 1 Stöð 1 Bíldshöfði 7 **RVK** , **bíll:** 40 40 Kristján **veður** skýað **aths.** **sérstök þjónusta:** 9 daši 1,00

sími: 4125102 **hiti:** 1,00 °C / 70,00 % **raki**

uppskrif 251 C50 mix loftlaust Beton **þjálni:** 10 **sigmál á vinnustað** 10 **veðrunarflokkur:** **hám. kornastærð:** 19 mm **styrkfráv.:.** meðal **yrkleikaflokkur:** C50flot læ lo **vinnanleiki:** **eftirmeðferð:** **þyngd:** 2,30 t.

eiginleikar:

	sement 1	sement 2	sement 3	fyllir	íblendi 1	íblendi 2	íblendi 2
Nafn framleiðandi	Kraftsement				Žjilniefni	Glenium sky	
vara nr.	2001				4002	4004	

tími	m³	fylliefni Björg	Sand 8	Raušamsandur	Björgperla		sement Kraftsement			fyllir	bæta við vatni Hreint vatn	Hreint vatn		raki		endurn.v fastefni	íblendi 1 Žjilniefni	Glenium sky	steypuhiti
framl	1,00	630kg	550kg	670kg	0kg	0kg	445kg	0kg	0kg	0kg	98kg	42kg	0kg	0kg	65kg	0,0kg	0,86 kg	4,00 kg	0,00kg
ppskr.	1,00	630kg	550kg	670kg	0kg	0kg	445kg	0kg	0kg	0kg	40kg	100kg	0kg	0kg	0kg	0,0kg	0,86 kg	4,00 kg	0,00kg
10:21	2,00	1310kg 4,0%	2460kg 4,0%	3830kg 2,5%	0kg	0kg	888kg	0kg	0kg	0kg	63kg	148kg	0kg	0kg	133kg	0,0kg	1,70 kg	9,70 kg	0,00kg
er	2,00	1310kg	1150kg	1370kg	0kg	0kg	888kg	0kg	0kg	0kg	63kg	85kg	0kg	0kg	133kg	0,0kg	1,70 kg	8,00 kg	0,00kg
beiðni	2,00	1313kg	1146kg	1374kg	0kg	0kg	890kg	0kg	0kg	0kg	63kg	84kg	0kg	0kg	0kg	0,0kg	1,72 kg	8,00 kg	0,00kg
raunv.(viðb.		1310kg	2460kg	3830kg	0kg	0kg	888kg	0kg	0kg	0kg	63kg	148kg	0kg	0kg			1,70 kg	9,70kg	0,00kg
beiðni (bæt		1313kg	2459kg	3833kg	0kg	0kg	890kg	0kg	0kg	0kg	63kg	147kg	0kg	0kg			1,72 kg	9,72kg	0,00kg
fráv.(viðb.)		-3kg	1kg	-3kg	0kg	0kg	2kg	0kg	0kg	0kg	0kg	1kg	0kg	0kg			-0,02 kg	-0,02kg	0,00kg
fráv.(viðb.)		-0,2 %	0,1 %	-0,1 %	0,0 %	0,0 %	-0,2 %	0,0 %	0,0 %	0,0 %	-0,1 %	0,7 %	0,0 %	0.0%			-1,2 %	-0,2 %	0,0 %
Ist/m³		655kg	575kg	685kg	0kg	0kg	444kg	0kg	0kg	0kg	32kg	43kg	0kg				0,85kg	4,00kg	0,00kg
Soll/m³		656kg	573kg	687kg	0kg	0kg	445kg	0kg	0kg	0kg	0kg	147kg	0kg				0,00kg	0,00kg	0,00kg
síló/dæla		3	2	1			1				2	2	0	0			2	4	

vatn: **viðbótarvatn:** 148 kg **grunnraki:** 133 kg **leiðr.-handbók:** 0 kg **leiðr.-pöntun:** 0 kg **Tara vatns:** 0 kg **V/S-umb.:** 0,31 **V/S-hám:** 0,55 **V/S-raun:** 0,32

GesamtGewicht: 4875 kg **rúmþyngd** ###########

framleiðslu kýrsla
prentað 23.2.2012 10:22

MC400_Bericht_Protokoll.rpt

bls.1/1

C. Anchor testing

Before the main experiment took place anchors were tested. The original purpose of this test was to evaluate longtime relaxation of the BFRP tendons. This test failed because of anchors failure, but the experience was used to develop anchors further. This first anchor type was made from Ø 16 mm threaded rod, with Ø 11 mm hole drilled 110 mm into the end and threaded for M 10, 70 mm in from the end (Figure 9-1). BFRP tendon was glued into the anchor with Hilti glue ("Klæbemørtel HIT-RE 500/330/1: Varenr.: 00305074," n.d.).

Figure 9-1 Ø 16 mm anchors

Anchor failed due to 47 kN force, which is about half of tendon ultimate tension strength. The anchor failed where its cross section area was smallest i.e. in the drilled section. Since the steel failed, not the glue, it was decided to have thicker steel in the anchors and make them from Ø 20 mm threaded rod. The procedure was otherwise identical to former test (Figure 9-2).

Figure 9-2 Testing anchors for BFRP tendons

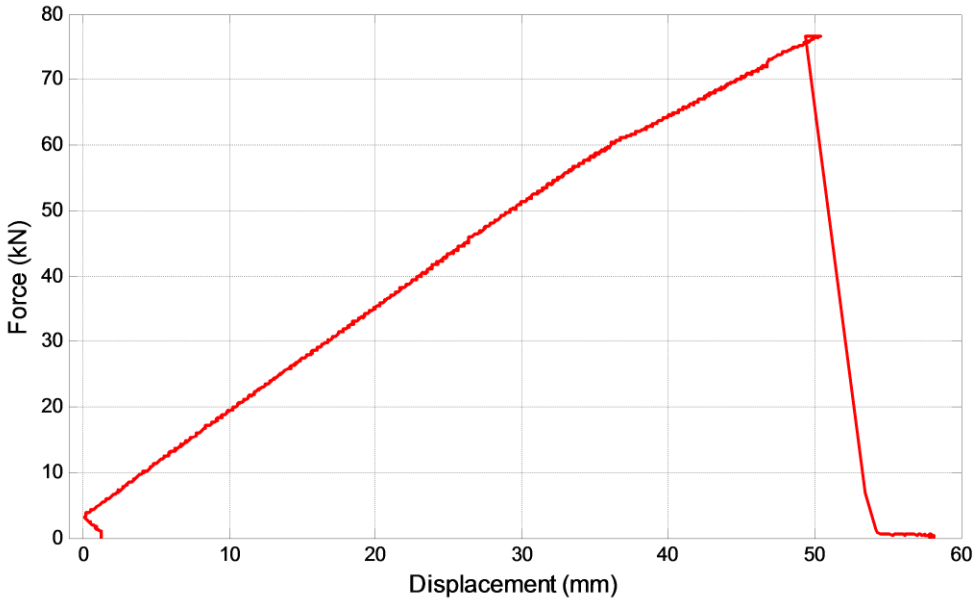

Figure 9-3 Force-displacement relationship for BFPR tendon

Anchor failed at 76 kN tension force, which is about 80% of the tendon ultimate tension strength. The failure was due to slipping between the anchor and tendon i.e. the glue failed. No further anchor tests were carried out, but anchors used in the main experiment were drilled 150 mm in and threaded 100 mm in from the end. This induces contact between the glue and the steel, and increases the surface in contact with the glue, which makes the anchor stand more tension force.

D. Strain gauge testing

In former experimental research carried out by Jónsson, 2011 BFRP tendon strain was measured with a strain gauge, glued to a 0,7 mm thick aluminum plate, which was glued to tendon (Figure 9-4, left).

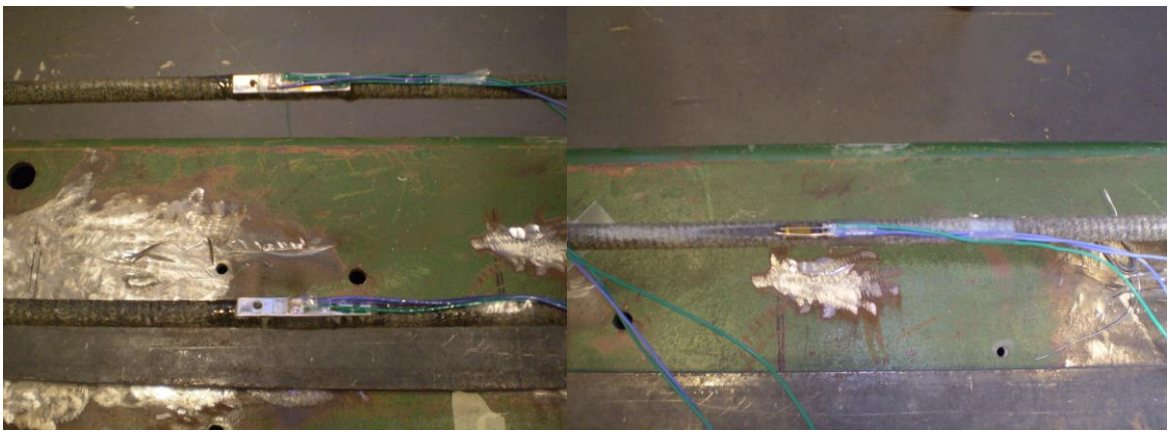

Figure 9-4 (Left) Gauges glued to aluminum plate that is glued to tendons (Right) Gauge glued directly to tendon

Sand-coated surface of the tendon was polished down with sandpaper under the aluminum plate.

To determinate the accuracy of these measurements and check, if the aluminum plate was necessary, an experiment was carried out. BFRP tendon with both strain gage on aluminum

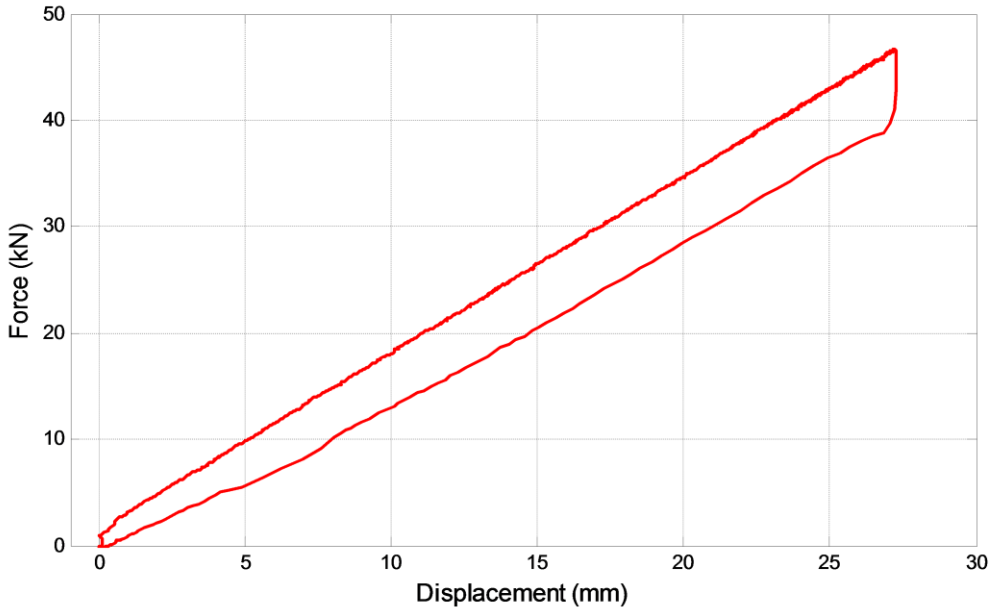

Figure 9-5 Force-displacement relationship for BFRP tendon

plate and gauge glued directly it (Figure 9-4, right) was stressed.

Maximum tension force was approximately 47 kN that is 50% of ultimate tendon strength.

To verify gauge measurements, strain according to Hookies' law, proportional to tendon elongation was calculated with the following equation: $\varepsilon = \frac{\Delta L}{L}$ where ΔL is tendon elongation and L is tendon length.

The difference between individual strain measurements can be seen in Figure 9-6.

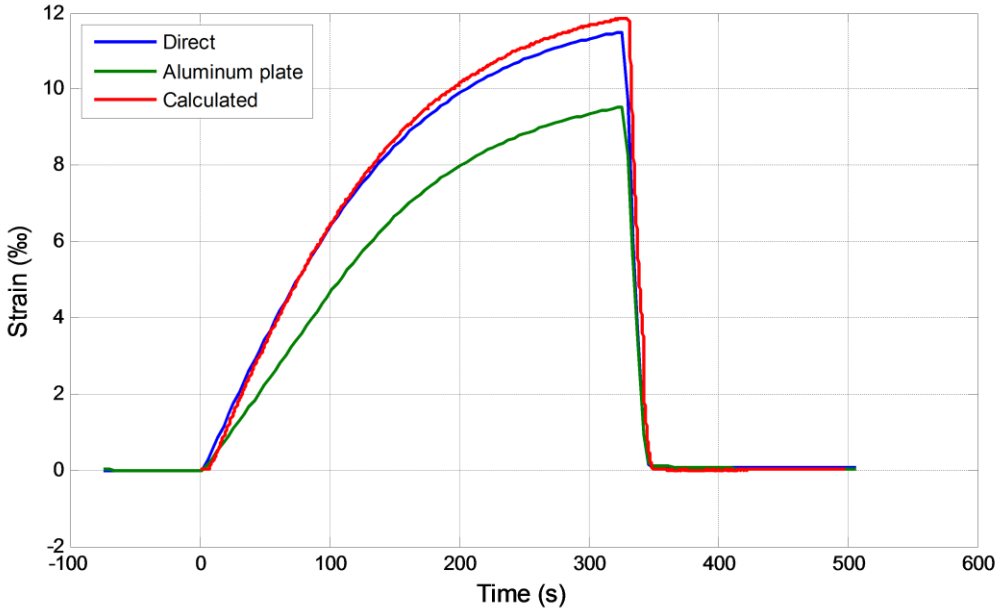

Figure 9-6 Tendon strain measured with different technique

Comparison shows that gauge glued directly to the tendon is accrued, with less than 4% error but gauge with aluminum plate underestimates tendon strain about 25%. This experiment showed that tendon strain can be measured directly with gauges. It should be noted that this was only one specimen and constant strain over tendon span is assumed.

E. Experimental work phases

The experimental work phases for beam specimens, in the performed work order are listed below:

BFRP tendons

- Eight BFRP 4 m long tendons were needed.
- BFRP tendons manufactured by "Magma Tech" were used (appendix A).

Anchors

- Eight Ø 20 mm, 270 mm long steel 8.8 threaded rods were needed and eight 730 mm long, to create the anchors.
- Ø 11 mm, 150 mm long hole was drilled into one end of all the rods.
- The holes of all rods were threaded inside with M 10 thread 100 mm in from the end.
- To induce contact between the steel and the glue, all surfaces in contact with glue were cleaned with strong oil cleaner.
- The holes in the rods were filled up with Hilti glue and some glue was put on the end of the tendons ("Klæbemørtel HIT-RE 500/330/1: Varenr.: 00305074," n.d.).
- The rods were installed on the ends of the tendons, 270 mm long rod on one end and 730 mm long on the other end.
- The glue was given several days to harden.
- A small surface on the BFRP tendons was polished with sandpaper to create a flat surface for the strain gauges.

Formwork

- Nearly 10 m^2 of oil coded, 16 mm thick plywood was needed for the formwork.
- The plywood was sawed into 200 mm strips for formworks sides and 232 mm for the downside.
- The bottom plates were screwed to the sideplates with woodscrews approximately c/c 150mm.
- Where individual plywood plates joined, another layer of plywood was screwed on the formworks sides.
- Two Ø 35 mm holes were drilled in the ends of each beams formwork, 50 mm from the lower edge and the sides.

- Eight steel washers h*b*t = 60*200*6 mm were cut down from a 6 mm thick steel strip.
- Two Ø 20 mm holes were drilled in the washers 50 mm from the ends and two Ø 4 mm holes, 5 mm from the ends.
- The washers were nailed to the formwork through the Ø 4 mm holes. The center of the Ø 20 mm holes in the washers was leveled 50 mm from formworks bottom, and sides.
- The surface of the formwork, in contact with concrete was lubricated with form oil.
- The BFRP tendons with anchors were laid through the end holes of the forms.
- Nuts were installed at the anchors' ends and the tendons were oriented so they would be centered after prestress. It was reckoned that the tendons would elongate 45 mm.
- Two plastic stars were installed on each BFRP tendon to hold them in place and keep concrete cover exact.
- The forms were installed in the prestress bench, leveled and fastened.
- RHS steel profiles were installed on the prestress bench and laid between the formwork to stiffen its sides. Those RHS profiles were welded to the angle shapes of the prestress bench.
- Nuts were installed at anchors' ends.
- Three plywood strips were laid across all four forms to stiffen them and keep them level. Those strips were screwed to the forms.
- 300 kg weight was installed on top of the RHS profiles to preclude them for buckling.

Strain gauge

- One strain gauge sensor was glued to the middle of each BFRP tendon.
- A small surface on the BFRP tendons was polished with sandpaper to create a flat surface for the strain gauges.
- The tendons were leveled and made sure that no tension force acted on them when gauges were glued on.
- The gauges were glued to the flat surface of the tendons with instant glue, which hardened in a few minutes. The gauges were oriented parallel to the tendons.
- Electrical vires were soldered to the gauges and threaded through Ø 6mm plastic tube out of the formworks lower edge and connected to measuring equipment.
- The gauges and their electrical wiring were wrapped with insulating tape and coated with a low modulus sealant to protect it from water ("Building Sealants," n.d.).

Prestress

- All anchors had nuts on their ends outside the prestress bench and another inside, to be used at transfer.
- All anchors on one site of the prestressing bench were long enough so they could lie through the hollow jack cylinder, which was used for stressing.
- Between the jack and bench was a 100 mm long Ø 100 mm steel tube with a section cut out along the curvature, big enough to tighten the anchor nut with a wrench.
- In the first round each tendon was jacked to a 25 kN prestress force and the anchor nut tightened to the prestress bench.
- The prestress force was 35 kN in the second round and 47 kN in final round.
- Strain in the tendons was measured while prestressing.

Casting

Concrete was bought from BM Vallá, a local concrete manufacturer. Target cylinder strength was 50 Mpa and maximum grain size 19 mm.

- 0,65 m^3 of concrete was needed.
- The concrete was transported with wheelbarrows from the concrete lorry, parked outside of the lab, and poured into the beam forms.
- To make sure that the concrete was compacted, it was picked in the formwork. This procedure was done very carefully around the strain gauges.
- When the formwork was full of concrete the top surface was leveled and smoothed.
- The top surface was watered 10 hours after casting and a couple of times a day for a week after.
- The top surface of the beams was covered with plastic sheets 10 hours after casting.
- Heat and humidity in the lab was measured while the concrete was curing. Measurements were taken once a day and the average heat was 20 degrees C and humidity 30%.

Cylinder specimen

Six cylinders were cast simultaneously with the beams. This specimen was done according to standard procedure (ÍST EN 12390-3).

- Six standard cylinder specimens Ø*h 100*200 mm were casted from the concrete mixture.
- The specimens were stored in the lab under the same conditions as the beams.
- Specimens were taken out of cylinders six days after casting and wrapped with cellophane and plastic sheet.
- Two and three days after beams 4 and 3 were tested a compression test was carried out for three cylinder specimens. This test was performed at ICI.
- Three other specimens were tested a couple of days after beams 1 and 2 were tested.
- The results can be seen in section (4.11).

Transfer

The prestress load was transferred from the prestress bench to the beams 24 days after casting.

- The inner nuts on the anchors were tightened to the beams and the outer nuts were untightened from the prestress bench.
- Strain in the tendons was measured at transfer.

Formwork taken of the beams

One day after transfer the formwork was taken off the beams and strain measurements stopped.

- The end part of the anchors was cut off. This part of the anchors wasn't necessarily for anchoring, just for the prestress.
- One of the L capes was untightened from the floor and moved away.
- The strain gauges were unplugged.
- The beams were mowed towards its loose end so the anchors were free of the prestress bench.
- The beams were lifted, one at a time with a forklift and the formwork removed from them. The beams were lifted on the ends and all movements were done very carefully.

Strain gauges

Three extra gauges were installed on each beam to measure the strain in the concrete at bending.

- Small surface was sanded to glue the gauges to.

- Two 30 mm long gauges were glued to the top face of the beams 50 mm from the sides at the middle.
- One 50 mm long gauge was glued to one side of the beams in level with the tendon, 50 mm from the lower edge.
- The gauges were laid in the exact longitudinal direction of the beams.
- The gauges on each beam were connected to a computer device while bending.

Bending test

Beam 4 was tested 29 days after casting, beam 3, 30 days, beam 1 and 2, 43 days.

- The beams were installed on the load bench "Hallgerður Langbók" with a forklift.
- They were positioned exactly and the load centered.
- A grid with 25 mm spacing, vertical and horizontal was drawn on the beams sides in the middle.
- The gauges were connected to the computer device that measured strain every 2 seconds and collected the data.
- Force and deflection was measured with a computer device that collected the data.
- The rotation speed on the hydraulic pump was kept as low as possible.
- After loading began, the beams were checked for flexural cracks, and when a crack reached 0,3 mm width the corresponding load was noted down.
- The beams were loaded until they failed.
- Displacement, force and time was measured automatically and collated.

External stirrups

- Beams 1 and 2 were fitted with twelve external steel stirrups. Six on each side.
- These stirrups consisted of UNP 65 steel profile on top of the beam and under, bolted together with two M 10 bolts.
- Six stirrups were on each side of the jack spaced 210 mm apart, and the first stirrup was located 500 mm from the end of the beams.

Nuts were tightened with a torch of 600 kg*cm.

F. Calculations

Calculation for load capacity of beams 1 and 2 in service condition (SLS) according to measured parameters of concrete. Calculations are explained in section (3.8).

f_{ck}	65,2	Mpa	Measured cylinder compressive strength of concrete
f_{ctm}	4,3	Mpa	Mean tensile strength of concrete
ΔP	20	%	Estimated loss of prestress force
P	94	KN	Prestress force
A	40000	mm^2	Cross-section area
e	50	mm	Tendons eccentricity
M_e	3,8E+6	Nmm	Moment due to tendons eccentricity
W	1,33E+06	mm^3	Section modulus
σ_{cp}	1,88	Mpa	Prestress
σ_e	2,82	Mpa	Stresses due to eccentricity
σ_0	9,00	Mpa	Stresses due to load
$\Sigma\sigma$	4,30	Mpa	Sum of stresses
M_o	12,0E+6	Nmm	Max. Moment in beam
F	15.000	N	Jack force
a	1600	mm	Shear span
F	**15,0**	**KN**	Jack force

Calculation for load capacity of beams 3 and 4in service condition (SLS) according to measured parameters of concrete. Calculations are explained in section (3.8).

f_{ck}	57,1	Mpa	Measured cylinder compressive strength of concrete
f_{ctm}	4,0	Mpa	Mean tensile strength of concrete
ΔP	20	%	Estimated loss of prestress force
P	94	KN	Prestress force
A	40000	mm^2	Cross-section area
e	50	mm	Tendons eccentricity
M_e	3,8E+6	Nmm	Moment due to tendons eccentricity
W	1,33E+06	mm^3	Section modulus
σ_{cp}	1,88	Mpa	Prestress
σ_e	2,82	Mpa	Stresses due to eccentricity
σ_0	8,70	Mpa	Stresses due to load
$\Sigma\sigma$	4,00	Mpa	Sum of stresses
M_o	11,6E+6	Nmm	Max. Moment in beam
F	14.500	N	Jack force
a	1600	mm	Shear span
F	**14,5**	**KN**	Jack force

Calculations of moment resistance according to (ACI 440.4R-04, 2004).

Parameters for concrete are chosen according to measurements.

$a := 1600$ mm Horizontally length from support to point load.

$h_{beam} := 200$ mm Beams high.

$b_{beam} := 200$ mm Beams width.

$A_c := h_{beam} \cdot b_{beam} = 40 \times 10^3$ mm^2 Beams cross-section area.

$d := 150$ mm Distance from top to tensile reinforcement.

$f_c := 65.2$ MPa Concrete compressive strength.

$\varepsilon_{cu} := 0.004$ Max. strain in concrete at compression.

$f_{pu} := 1200$ MPa Ultimate tensile strength of the fiber.

$E_p := 50000$ MPa Fibers elastic modulus.

$A_p := 157$ mm^2 Fibers cross-section area.

$\varepsilon_{pu} := 0.026$ Ultimate strain in fibers at tension.

$\varepsilon_{pe} := 0.011$ Strain in fibers due to prestress.

$$\beta_1 := 0.85 - \left(\frac{f_c - 27.5}{6.9} \cdot 0.05 \right) = 0.577$$ Adjusting β1 factor for the concretes strength.

$$\rho := \frac{A_p}{b_{beam} \cdot d} = 5.233 \times 10^{-3}$$ Reinforcement ratio.

$$\rho_b := 0.85 \cdot \beta_1 \cdot \frac{f_c}{f_{pu}} \cdot \frac{\varepsilon_{cu}}{\varepsilon_{cu} + \varepsilon_{pu} - \varepsilon_{pe}} = 5.608 \times 10^{-3}$$ (3 – 6)
Balanced reinforcement ratio.

Tension-controlled section: $\rho<\rho_b$

Ultimate moment capacity of the section.

$$M_n := \rho \cdot b_{beam} \cdot d^2 \cdot f_{pu} \cdot \left(1 - \frac{\rho}{1.7} \cdot \frac{f_{pu}}{f_c}\right) = 26.7 \times 10^6 \quad \text{kNm}$$

$$F_{ult} := \frac{M_n \cdot 10^{-3} \cdot 2}{a} = 33.3 \quad \text{kN} \quad \text{Ultimate force.}$$

Calculations of moment resistance with methods from (O'Brien et al., 2012) according to (EN 1992-1-1, 2004). Parameters for concrete are chosen according to measurements.

$a :=$	1600	mm	Horizontally length from support to point load.
$h_{beam} :=$	200	mm	Beams high.
$b_{beam} :=$	200	mm	Beams width.
$A_c := h_{beam} \cdot b_{beam} = 40 \times 10^3$		mm^2	Beams cross-section area.
$d :=$	150	mm	Distance from top to tensile reinforcement.
$e_f :=$	50		Eccentricity of tendon.
$P :=$	94200	N	Prestress force.
$\rho :=$	0.80		Effective ratio of prestress.
$E_f :=$	50000	MPa	Fibers elastic modulus.
$f_{fu} :=$	1200	N/mm^2	Ultimate tensile strength of the fiber.
$A_f :=$	157	mm^2	Fibers cross-section area.
$E_c :=$	38600	MPa	Concretes modulus of elasticity.
$f_c :=$	65.2	MPa	Concrete compressive strength.
$\varepsilon_{cu} :=$	0.004		Max. strain in concrete at compression.

$I_g := \frac{1}{12} \cdot h_{beam} \cdot b_{beam}^{3} = 133 \times 10^{6}$ mm4 Sections moment of inertia.

$\varepsilon_{ce} := \frac{1}{E_c} \cdot \left(\frac{\rho \cdot P}{A_c} + \frac{\rho \cdot P e_f^{2}}{I_g} \right) = 75 \times 10^{-6}$ Strain in concrete due to tendons eccentricity.

$X := 25.1$ mm Distance from top to sections neutral axis.

$\varepsilon_{ct} := \frac{-\varepsilon_{cu} \cdot (d - X)}{X} = -0.02$ Concretes strain at tension.

$\varepsilon_{fu} := \frac{-\rho \cdot P}{A_f \cdot E_f} - |\varepsilon_{ct}| - |\varepsilon_{ce}| = -0.03$ Strain in the fibers.

$F_f := A_f \cdot E_f \cdot |\varepsilon_{fu}| = 223 \times 10^{3}$ N Tension force in the fibers.

$F_c := 0.8 \cdot X \cdot b_{beam} \cdot 0.85 \cdot f_c = 223 \times 10^{3}$ N Compression force in the concrete.

$M_{ult} := F_f \cdot (d - 0.4 \cdot X) = 29.3 \times 10^{6}$ Nmm Ultimate moment capacity of the section.

$F_{ult} := \frac{M_{ult} \cdot 10^{-3} \cdot 2}{a} = 36.6$ kN Ultimate force.